AD 745903

MAGNETIC RARE EARTH COMPOUNDS II

Hewlett-Packard Company

Palo Alto, California 94304

FINAL TECHNICAL REPORT

June 1972

Contract No. DAAH01-71-C-1259
Program Code No. OD10

(This contract will be continued under contract No. DAAH01-72-C-0996)

DDC
JUL 25 1972

ARPA Support Office
Research, Development, Engineering,
and Missile Systems Laboratory
U.S. Army Missile Command
Redstone Arsenal, Alabama

A Research Project Sponsored by the Advanced Research Projects Agency, Department of Defense, Washington, D.C., ARPA Order 1627

88

ACCESSION for
CFSTI WHITE SECTION
DDC BUFF SECTION
UNANNOUNCED
JUSTIFICATION
BY
DISTRIBUTION/AVAILABILITY CODES
Dist.
A

NOTICE

"This research was sponsored by the Advanced Research Projects Agency of the Department of the Defense under ARPA Order 1627 and was monitored by the US Army Missile Command under Contract Number DAAH01-71-C-1259. Views and conclusions expressed herein are the primary responsibility of the author or the contractor and should not be interpreted as representing the official opinion or policy of USAMICOM, ARPA, DOD or any other agency of the Government."

Unclassified
Security Classification

DOCUMENT CONTROL DATA - R&D

(Security classification of title, body of abstract and indexing annotation must be entered when the overall report is classified)

1 ORIGINATING ACTIVITY *(Corporate author)*

Hewlett-Packard Company
1501 Page Mill Road
Palo Alto, California 94304

2a REPORT SECURITY CLASSIFICATION

Unclassified

2b GROUP

3 REPORT TITLE

MAGNETIC RARE EARTH COMPOUNDS

4 DESCRIPTIVE NOTES *(Type of report and inclusive dates)*

Final Technical Report (June 14, 1971 to June 13, 1972)

5 AUTHOR(S) *(Last name, first name, initial)*

Burmeister, Robert A.
Hiskes, Ronald

6 REPORT DATE	7a. TOTAL NO. OF PAGES	7b NO OF REFS
July 1972	80	30

8a CONTRACT OR GRANT NO.

DAAH01-71-C-1259

b PROJECT NO.

Technical Requirement No. 1335

c Program Code No. 0D10

d ARPA Order No. 1627

9a. ORIGINATOR'S REPORT NUMBER(S)

9b. OTHER REPORT NO(S) *(Any other numbers that may be assigned this report)*

10 DISTRIBUTION STATEMENT

Approved for public release; distribution unlimited.

11 SUPPLEMENTARY NOTES

12. SPONSORING MILITARY ACTIVITY

Advanced Research Projects Agency
Department of Defense,
Washington, D.C., ARPA Order 1627

13 ABSTRACT

The magnetically uniaxial rare earth garnets $(Eu,Er)_3(Ga,Fe)_5O_{12}$ and $(Gd,Y,Yb)_3(Ga,Fe)_5O_{12}$ have been grown on {111} $Gd_3Ga_5O_{12}$ substrates by the liquid phase epitaxial dipping technique in both $PbO-B_2O_3$ and $BaO-B_2O_3-BaF_2$ solvents.

The BaO-based solvent has been characterized with respect to solubility and suitable growth parameters of the magnetic garnets. The results indicate that the BaO-based solvent has many significant advantages over the commonly used $PbO-B_2O_3$ solvent.

The substrate and magnetic films have been characterized with respect to compositional uniformity, lattice parameters, impurities, surface morphology, thickness uniformity and magnetic properties. The composition best suited to magnetic bubble devices found to date has been $Gd_{0.7}Y_{1.55}Yb_{0.75}Ga_{0.9}Fe_{4.1}O_{12}$ (solution composition) which exceeds all the device requirements except that of temperature stability.

A comparison of magnetic films of similar composition grown in the PbO-based and BaO-based solvents (at different temperatures) indicates that the films are of comparable quality, and the demonstrated superiority of the BaO-based solvent makes it advantageous for the growth of the magnetic bubble garnets.

DD FORM 1 NOV 65 1473 REPLACES DD FORM 1473, 1 JAN 64, WHICH IS OBSOLETE FOR ARMY USE.

Unclassified
Security Classification

Unclassified

Security Classification

14. KEY WORDS	LINK A ROLE	LINK A WT	LINK B ROLE	LINK B WT	LINK C ROLE	LINK C WT
Garnets						
Rare Earths						
Magnetic Bubbles						
Liquid Phase Epitaxy						
BaO-based Solvents						
Crystal Growth						

14

Unclassified

Security Classification

TECHNICAL REQUIREMENT NO. 1335
ARPA Order 1627

MAGNETIC RARE EARTH COMPOUNDS

FINAL TECHNICAL REPORT

June 1972

DISTRIBUTION STATEMENT A
Approved for Public Release;
Distribution Unlimited

HEWLETT-PACKARD COMPANY
Palo Alto, California
94304
(415) 493-1501
Contract No. DAAH01-71-C-1259
Program Code No. 0010

Monitored By
ARPA Support Office
Research, Development, Engineering, and
Missile Systems Laboratory
U.S. Army Missile Command
Redstone Arsenal, Alabama

Approved for Public Release
Distribution Unlimited

A Research Project Sponsored by the Advanced
Research Projects Agency, Department of
Defense, Washington, D. C., ARPA Order 1627

10

FOREWORD

This report describes work performed under Contract DAAH01-71-C-1259 for the ARPA Support Office, Research, Development, Engineering, and Missile Systems Laboratory, U.S. Army Missile Command, Redstone Arsenal, Alabama during the period June 14, 1971 through June 13, 1972. The monitor for this project was S. L. Johnston. The work was performed in the Solid-State Laboratory of Hewlett-Packard Laboratories under the direction of P. E. Greene. The work was supervised by R. A. Burmeister, and this report was written by R. Hiskes. The assistance of R. Baugh, R. Clover, L. Cutler, R. L. Lacey and P. Waites of the Physical Research Laboratory of Hewlett-Packard Laboratories for the design and interpretation of much of the magnetic characterization is gratefully acknowledged.

SUMMARY

The magnetically uniaxial rare earth garnets $(Eu,Er)_3(Ga,Fe)_5O_{12}$ and $(Gd,Y,Yb)_3$ $(Ga,Fe)_5O_{12}$ have been grown on {111} $Gd_3Ga_5O_{12}$ substrates by the liquid phase epitaxial dipping technique in both $PbO-B_2O_3$ and $BaO-B_2O_3-BaF_2$ solvents in the temperature range of 900°C-1040°C.

The BaO-based solvent has been characterized with respect to solubility and suitable growth parameters of the magnetic garnets. The results indicate that the BaO-based solvent has many significant advantages over the commonly used $PbO-B_2O_3$ solvent.

The substrate and magnetic films have been characterized with respect to compositional uniformity, lattice parameters, impurities, surface morphology, thickness uniformity and magnetic properties. New optical techniques have been developed for the determination of film thickness and intrinsic coercive force. The composition $Gd_{0.7}Y_{1.55}Yb_{0.75}Ga_{0.9}Fe_{4.1}O_{12}$ exceeds all the magnetic bubble device requirements except that of temperature stability. 3.5 μm thick films of this composition have been reproducibly grown with a characteristic length $\ell \sim 0.8$ μm, $4\pi M_s \sim 130$ gauss, $\mu > 500$ cm/Oe-sec, $H_c < 0.05$ Oe, $H_K \sim 900$ Oe, and with defect free areas greater than 20 mm^2. These films exhibit a new type of bubble domain, termed the "hard" bubble, which does not obey the classical bubble stability theory and which can be produced or eliminated at will. A model has been proposed for the formation of "hard" bubbles.

A comparison of magnetic films of similar composition grown in the PbO-based and BaO-based solvents (at different temperatures) indicates that the films have comparable magnetic properties and the superiority of the BaO-based solvent in other respects makes it advantageous for the growth of the magnetic bubble garnets.

TABLE OF CONTENTS

Section	Title	Page
1.0.	INTRODUCTION	1
2.0.	CRYSTAL GROWTH	5
2.1.	Introduction	5
2.1.1.	Control of Liquid Phase Epitaxial Crystal Growth	5
2.1.2.	Garnet Composition and Substrate Selection	8
2.1.3.	Solvent Requirements	9
2.2.	Experimental Procedures	12
2.2.1.	Characterization of the $BaO-BaF_2-B_2O_3$ Solvent	12
2.2.2.	Substrate Preparation	16
2.2.2.1.	Boule and Substrate Processing	16
2.2.2.2.	Substrate Characterization and Evaluation	16
2.2.3.	Crystal Growth	24
2.2.3.1.	Growth in BaO-based Solvents	24
2.2.3.1.1.	Results and Discussion of Growth in BaO-based Solvents	26
2.2.3.2.	Results of Growth in PbO-based Solvents	30
3.0.	CHARACTERIZATION AND EVALUATION	34
3.1.	Film Surface Morphology and Magnetic Defect Density	34
3.2.	Film Composition and Impurity Analyses	38
3.3.	Lattice Parameter Determination	42
3.4.	Film Thickness Measurement	45
3.5.	Static Domain Measurements	47
3.6.	Magnetization and Anisotropy Energy	49
3.7.	Domain Wall Mobility	49
3.7.1.	Dynamic Bubble Collapse	49

TABLE OF CONTENTS

Section	Title	Page
3.7.2	Stripe Domain Response to Applied Field	50
3.8.	Coercive Force	52
3.9.	Néel Temperature Measurement	56
3.10.	Temperature Coefficient of Magnetic Properties	60
3.11.	Results and Discussion of Magnetic Measurements. . . .	64
4.0.	CONCLUSIONS	73
	REFERENCES	74

LIST OF ILLUSTRATIONS

Figure	*Title*	*Page*
Figure 1.	Approximate Liquidus Points for the $BaO-B_2O_3-BaF_2$ System (the points represent approximate temperatures at which a large qualitative increase in viscosity was noted).	13
Figure 2.	Approximate solubility curve for $EuEr_2Ga_{0.7}Fe_{4.3}O_{12}$ in 41 (mole)% BaO, 41% B_2O_3, 18% BaF_2.	15
Figure 3.	Strain fields caused by dislocations in $Gd_3Ga_5O_{12}$ substrate. (Transmitted polarized light, 200X).	19
Figure 4.	Dislocation etch pits in a <111> $Gd_3Ga_5O_{12}$ substrate. Upper photo is the top surface of substrate, lower photo is the same area on the bottom surface. (200X)	20
Figure 5.	Lang transmission topograph of a thin (110μm) <111> $Gd_3Ga_5O_{12}$ substrate containing a "core" defect. (220) reflection, MoKα radiation, 5.3X.	21
Figure 6.	Scanning reflection topograph of an epitaxial film of $Gd_{0.79}Y_{1.46}Yb_{0.75}Fe_{4.1}Ga_{0.9}O_{12}$ grown on a cored substrate. (888) reflection, CuKα radiation, 6X.	22
Figure 7.	Scanning reflection topograph of a core free, dislocation free <111> $Gd_3Ga_5O_{12}$ substrate. (888) reflection, CuKα radiation, 6X.	23
Figure 8.	Apparatus for Epitaxial Crystal Growth of Magnetic Bubble Garnets.	25
Figure 9.	Growth rate of $Gd_{0.7}Y_{1.55}Yb_{0.75}Ga_{0.9}Fe_{4.1}O_{12}$ at 990°C in $BaO-B_2O_3-BaF_2$ solvent.	29
Figure 10.	Growth rate of $(Gd,Y,Yb)_3(Fe,Ga)_5O_{12}$ at 900°C in $PbO-B_2O_3$ solvent.	33
Figure 11a.	Surface morphology of $Gd_{0.7}Y_{1.55}Yb_{0.75}Ga_{0.9}Fe_{4.1}O_{12}$ grown on $Gd_3Ga_5O_{12}$ in $BaO-B_2O_3-BaF_2$ solvent after adhered solution has been etched off.	36
Figure 11b.	Surface morphology of $Gd_{0.7}Y_{1.55}Yb_{0.75}Ga_{0.9}Fe_{4.1}O_{12}$ grown on $Gd_3Ga_5O_{12}$ in $BaO-B_2O_3-BaF_2$ solvent with slow withdrawal from soltuion.	36

LIST OF ILLUSTRATIONS

Figure	*Title*	*Page*
Figure 12.	As grown $Gd_{0.7}Y_{1.55}Yb_{0.75}Ga_{0.9}Fe_{4.1}O_{12}$ epitaxial film grown on $Gd_3Ga_5O_{12}$ from a $PbO-B_2O_3$ growth solution.	36
Figure 13.	The growth rate dependence of lead content in $(Eu,Er)_3$ $(Ga,Fe)_5O_{12}$ epitaxial layers grown by the cooling technique from 900 to 850°C.	40
Figure 14.	Concentration of lead and barium incorporated in $(Eu,Er)_3$ $(Ga,Fe)_5O_{12}$ and $(Eu,Y)_3$ $(Fe,Ga)_5O_{12}$ during LPE growth.	41
Figure 15.	Variation of lattice parameter with solution composition for garnet films grown in $BaO-BaF_2-B_2O_3$ solvent in the temperature range 900-1040°C.	43
Figure 16.	Variation of lattice parameter with solution gallium content for films grown in $PbO-B_2O_3$ solvent at 900°C.	44
Figure 17.	Apparatus for measuring film thickness.	46
Figure 18.	Typical fringe patterns in $(Gd,Y,Yb)_3$ $(Fe,Ga)_5O_{12}$ 3.6 μm thick grown in $BaO-BaF_2-B_2O_3$ solvent. Na illumination (λ = 5890Å). The faint very narrow fringes near the center of the sample (if visible) are caused by interference between the front surface of the film and the back surface of the substrate.	48
Figure 19.	Experimental configuration for mobility measurements.	51
Figure 20.	Apparatus for coercive force and Neél temperature measurements.	55
Figure 21.	Neél temperature as a function of solution gallium content for $(Gd,Y,Yb)_3$ $Ga_xFe_{5-x}O_{12}$ grown at 900°C in $PbO-B_2O_3$ solvent.	57
Figure 22.	Variation of the Neél temperature transition region with epitaxial layer thickness.	59

LIST OF ILLUSTRATIONS

Figure	*Title*	*Page*
Figure 23.	Temperature dependence of magnetization and characteristic length for $Gd_{0.7}Y_{1.55}Yb_{0.75}Ga_{0.9}Fe_{4.1}O_{12}$ grown in $BaO-B_2O_3-BaF_2$ solvent.	61
Figure 24.	Temperature dependence of the product of the exchange constant A times the anisotropy constant K for $Gd_{0.7}Y_{1.55}Yb_{0.75}Ga_{0.9}Fe_{4.1}O_{12}$ grown in $BaO-B_2O_3-BaF_2$ solvent.	62
Figure 25.	Quasi-static operating margins for $Gd_{0.7}Y_{1.55}Yb_{0.75}Ga_{0.9}Fe_{4.1}O_{12}$ Grown in $BaO-B_2O_3-BaF_2$ Solvent. (3μm spacing between T-bars and garnet surface).	64
Figure 26.	Dependence of bubble diameter upon bias field for Thiele type and hard type bubbles.	68
Figure 27a.	Domain structure in $Gd_{0.7}Y_{1.55}Yb_{0.75}Ga_{0.9}Fe_{4.1}O_{12}$. Zero bias field (200X).	69
Figure 27b.	Domains have been cut and bias field increased to 20 Oe. (200X)	69
Figure 27c.	Bias field 30 Oe. (200X)	69
Figure 27d.	Bias field 40 Oe (200X)	70
Figure 27e.	Bias field 53 Oe (200X)	70
Figure 27f.	Bias field increased to 65 Oe to pop most bubbles, then reduced to 28 Oe. (200X)	70
Figure 28.	Proposed model for the domain wall structure of hard bubbles. Arrows represent the component of spin in the plane of a bubble film.	72

LIST OF TABLES

Table	Title	Page
Table I.	Materials Specifications for Magnetic Bubble Devices	2
Table II.	Properties of PbO-based and BaO-based Solvents	11
Table III.	Growth Parameters for LPE Garnet Growth in $BaO-B_2O_3-BaF_2$ Solvent	27
Table IV.	Growth Parameters for $(Gd,Y,Yb)_3(Ga,Fe)_5O_{12}$ Grown in $PbO-B_2O_3$ Solvent	32
Table V.	Characterization Techniques for Magnetic Rare Earth Garnets	35
Table VI.	Properties of Epitaxial Layers Grown in $BaO-B_2O_3-BaF_2$ and $PbO-B_2O_3$ Solvents	53
Table VII.	Comparison of the Properties of Rare Earth Bubble Garnets Grown in BaO-Based and PbO-Based Solvents	66

SECTION I

1.0. INTRODUCTION

The growth of magnetic bubble technology has been rapid ever since the basic features of this technology were first demonstrated in the orthoferrites,[1] and more recently in the rare earth garnets.[2] Bubble devices utilize mobile cylindrical domains contained in thin films of these materials. To ensure proper response of the magnetic bubbles to applied magnetic forces, the films must be of uniform composition and thickness, and must be free of most common crystallographic imperfections. Epitaxial liquid phase and vapor phase growth techniques on paramagnetic transparent substrates have proved successful in providing material meeting most of the device specifications shown in Table 1.

At this time, however, materials problems are still a major limitation to the practical utilization of bubble devices. In view of the technological importance of these devices and the key role of magnetic rare earth compounds, this program was undertaken in an effort to advance the state-of-the-art in the science and technology of these materials. The specific objectives of this program include the following:

1. Development of practical techniques for the growth of single crystals of rare earth compounds having properties suitable for studies and utilization of magnetic domain wall phenomena.
2. Acquisition of the necessary data to better characterize and quantitatively describe both the crystal growth process and the salient physical and chemical properties of the crystals produced.

TABLE I

Materials Specifications for Magnetic Bubble Devices

D	6 μm (bias field dependent)	Bubble Diameter
ℓ	0.8 μm†	Characteristic Length
$4\pi M_s$	150 Gauss†	Saturation Magnetization
h	3.5 μm†	Thickness
μ	> 200 cm/Oe-sec	Mobility
H_c	< 0.3 Oe	Coercive Force
Defect Density	< 5/cm^2	Crystal defects which affect magnetic properties
Usable Defect Free Area	> 10 mm^2	"
H_k	> 2 · ($4\pi M_s$)	Anisotropy Field
$\left.\frac{d\ell}{dT}\right)_{298°K}$	<0.01 μm/°K	Temperature coefficient of characteristic length
$\varepsilon = \frac{2\,(r_a - r_b)}{(r_a + r_b)}$	<0.2	Bubble Ellipticity

† ℓ, $4\pi M_s$ and h to have ±1% variation over the surface in a given run and to be reproducible to within 5% from run to run.

3. Determination of the relationship between methods and parameters of the crystal growth process and relevant physical properties of the crystals thus grown.

To meet these objectives, we have developed a new solvent, comprised of BaO, B_2O_3 and BaF_2 for the solution growth of these compounds as well as explored the limitations of conventional PbO-based solvents. The choice of materials to be grown in these solvents has been dictated by the current state-of-the-art knowledge of the magnetic bubble materials.

In the previous contract, $YFeO_3$ was chosen as the initial material to be studied since it is typical of the rare earth orthoferrites, and during that program single crystals of $YFeO_3$ were grown and characterized.[3,4] At the beginning of this program, we investigated the liquid phase epitaxial (LPE) growth of $YFeO_3$ on $YAlO_3$, but the large lattice parameter mismatch and the considerable substrate attack by the growth solution precluded successful heteroepitaxial growth in this system.

Shortly after the initial reports of the possibility of preparing uniaxial rare earth garnet bubble materials,[2] we initiated studies of the LPE growth of these garnets, such as $Eu_2Er_1Ga_{0.7}Fe_{4.3}O_{12}$ and $Eu_1Er_2Ga_{0.7}Fe_{4.3}O_{12}$, which exhibit the necessary uniaxial anisotropy with the proper stable bubble size of 5-10 microns.[4,5] More recently in this program we have investigated epitaxial growth of the rare earth garnets having the composition $(Gd,Y,Yb)_3(Fe,Ga)_5O_{12}$ in both BaO-based and PbO-based solvents in order to directly compare the two solvents.

In the body of the report, the crystal growth procedures developed for the bubble garnets in both the BaO-based and PbO-based solvents will be described, the characterization and properties of the BaO-based solvent will be discussed, and the physical, chemical and magnetic properties of the epitaxial films grown in these solvents will be described.

SECTION II

2.0. CRYSTAL GROWTH

2.1. Introduction

Although rare earth orthoferrites and garnets have been grown by a variety of techniques,[6] the most promising method for materials to be used for magnetic bubble device applications has been that of epitaxial growth on a paramagnetic transparent substrate, including both liquid phase epitaxial (LPE)[7-14] and vapor phase epitaxial (VPE) growth (also referred to as chemical vapor deposition (CVD)).[15-20] We have chosen LPE because it is an inherently simple and reliable process when used with a stable solvent, and one which permits precise interface temperature and temperature gradient control when properly implemented. The as-grown geometry (thin film on a supporting substrate) is ideal for device use, and the growth temperature is lower than that required for VPE, which minimizes thermal stress upon cooling to room temperature.

2.1.1. Control of Liquid Phase Epitaxial Crystal Growth

The growth process is one of the most critical factors influencing the magnetic properties of the epitaxial layer. Proper control of the process involves a quantitative understanding of the relationships between the crystal morphology, composition and perfection, and the solid-liquid interface variables. These variables include the interface temperature and composition, the liquidus temperature of the solution at the interface composition, the velocity and shape of the growing crystal, and the nature of

the solute, thermal and momentum boundary layers ahead of the interface. The quantitative relationships between these interface variables and the controllable macroscopic variables of the growth system must be developed, primarily through the solution of the boundary value problems involved (many of which have not been solved). The controllable variables are the solution temperature and composition far from the interface, the cooling rate or degree of initial supersaturation, the shape of the container holding the solution, the amount and type of fluid motion, and the nature of the substrate.

The quantitative solution of the boundary value problems involves a knowledge of many of the material parameters of the system, which is practically nonexistent for the rare earth systems. Some of these parameters are listed below:

(i) Parameters related to phase equilibria such as the latent heat of fusion of the crystal, melting point of the solvent, solute equilibrium distribution coefficients and the slope of the liquidus curve of the system.

(ii) Nucleation data such as the critical undercooling needed for heterogeneous nucleation.

(iii) Transport parameters including diffusion coefficients of all species present in both solid and liquid, as well as their interface partition coefficients and site preference coefficients in the crystal.

(iv) Quantities needed for the solution of the hydrodynamic equations such as the viscosity and density of the solution.

(v) The energetic parameters, such as the solid/liquid interfacial energy, entropy of fusion, and the distribution and energy of imperfections.

(vi) Thermal transport data including thermal conductivities and diffusivities of the solid and liquid.

The determination of these parameters would entail in many cases a tedious series of experiments. What can more easily be accomplished, however, is a semi-empirical correlation of the controllable macroscopic variables (enlightened by an awareness of the relationships outlined above) with the observed properties of the crystals produced. We have emphasized this approach in the present program. In order to consistently produce rare earth garnets by the liquid phase epitaxial technique meeting the specifications in Table I, the following variables must be controlled.

(i) The solution compositional uniformity and homogeneity from run to run and during the run must be controlled as precisely as possible by careful initial weighing of ingredients and vigorous prolonged stirring of the solution at temperatures at least 100°C above the liquidus temperature. The PbO lost by vaporization should be replaced after each growth run.

(ii) The growth temperature and cooling rate must be held constant from run to run to within ±0.5% and ±0.1°C/min. respectively.

(iii) The boundary layers must be kept constant from run to run as well as spatially during each run by controlling the fluid motion. This is accomplished by maintaining the solution isothermal to ± 0.5°C.

2.1.2. Garnet Composition and Substrate Selection

Garnet compositions must be carefully selected to meet the stringent materials requirements listed in Table I, and perhaps the most critical control is needed in matching substrate and epitaxial layer lattice parameters. Although this match has in some cases been met by forming solid solutions, such as $Gd_3Ga_5O_{12}$, with either $Nd_3Ga_5O_{12}$, $Sm_3Ga_5O_{12}$, or $Dy_3Ga_5O_{12}$ to raise or lower the lattice parameter of the substrate respectively, the majority of the bubble garnets (including those produced in this program) have been grown on $Gd_3Ga_5O_{12}$ since this material is available in the quantity and quality needed for epitaxial growth.

Two rare earth garnet compositions were studied during the current contract period, the range of compositions represented by $(Eu,Er)_3(Ga,Fe)_5O_{12}$ and more recently $(Gd,Y,Yb)_3(Fe,Ga)_5O_{12}$, for several reasons; (i) they exhibit mobile bubble domains at reasonable values of magnetic bias and drive fields, (ii) they can be grown on $Gd_3Ga_5O_{12}$ substrates, and (iii) these combinations of epitaxial layers and substrate are representative of the rare earth bubble garnet growth process. The evaluation of techniques for proper growth and characterization of these garnets is germane to the entire class of rare earth garnets, and attention can thus be shifted to any other compositions deemed more technologically desirable at any point in the program without loss of continuity to the project.

2.1.3. Solvent Requirements

There are certain basic solvent requirements desirable for liquid phase epitaxial crystal growth of the rare earth garnets which are enumerated below:

1. Low vapor or dissociation pressure and low reactivity with the crucible at crystal growth temperatures is desirable, in order to avoid changes in liquid level and composition.
2. The solvent should have a high solubility for the crystal growth constituents, and the metastable supercooled solution should be stable at large supercoolings for heteroepitaxial growth in order to inhibit initial substrate dissolution before epitaxial growth begins.
3. The liquidus curve (temperature versus composition) should be steep to permit precise control of supersaturation by controlling the solution temperature.
4. The distribution coefficients of the crystal constituents should not vary with temperature to prevent spurious composition fluctuations due to temperature excursions and uneven temperature distribution in the solution during growth.
5. The distribution coefficients as well as the solubility of the solvent ions in the crystal must be very low to prevent solvent incorporation during growth. This effect can lead to significant changes in composition and lattice parameter in the epitaxial layer.

6. It is desirable for the compound to be congruently saturating to enhance stoichiometric growth and deter the formation of other phases.
7. The solvent should have both a low melting point and low viscosity to permit growth at as low a temperature as possible.
8. The solvent must wet the substrate and growing crystal, but should also be readily removable from the epitaxial layer after growth.
9. The solution should be readily soluble in common solvents that do not attack the crystal or the growth crucible to facilitate cleaning operations.
10. The solvent should be inexpensive and readily obtainable in high purity form.

It is desirable to tailor the solvent to the crystal being grown to satisfy as many of these requirements as possible. In this program we are evaluating two classes of solvents, the PbO-based and the BaO-based solvents. The commonly used $PbO-B_2O_3$ solvents fail in requirements 1, 4,5 and 6. The BaO-based solvents, on the other hand, have been found to fulfill all the listed requirements, although the PbO-based solvent appears to have a minor advantage in requirements 7 and 8. A comparison between the two solvents is shown in Table II, and the data listed there are discussed more fully in the next section.

TABLE II

Properties of PbO-based and BaO-based Solvents

	$BaO-B_2O_3-BaF_2$	$PbO-B_2O_3$
Melting Point	750 - 915°C	< 700°C
Volatility	Negligible at 1450°C	Considerable at 900°C
Viscosity	Relatively high at temperatures less than 1050°C, increases with time at temperatures less than 850°C, > 100 cp	Low down to 800°C, 10-100 cp
Chemical Reactivity with Platinum	Negligible	Reacts readily if free lead is present
Density	Less than magnetic bubble materials (~ 4.7 gm/cm^3)	Greater than magnetic bubble materials (~ 6 gm/cm^3)
Solubility of Magnetic Garnets	~ 18 mole % at 1000°C, 2-3 times greater than $PbO-B_2O_3$ solvent	~ 7.3 mole % at 940°C
Phase Stability	Garnets and orthoferrites are congruently saturating	Garnets are not congruently saturating
Solvent Incorporation (Decreases with increasing temperature)	<0.1 wt. % Ba at typical crystal growth temperatures	1-3 wt. % Pb at 900°C growth temperature
Temperature Variation of Distribution Coefficients	$\alpha_{Ga} \approx 1$, temperature insensitive	$\alpha_{Ga} = 1.6 - 2.5$, very temperature sensitive
Toxicity	Slight unless ingested	Fumes of PbO are very toxic

2.2. Experimental Procedures

2.2.1. Characterization of the $BaO-BaF_2-B_2O_3$ Solvent

Many of the properties of this solvent have been described previously,[3,4,5] and the discussion here will only summarize the results of those experiments which were completed during previous report periods. Solvent compositions were prepared by in situ thermal decomposition of a mixture of $BaCO_3$, B_2O_3 and BaF_2.* Approximate melting point data (shown in Figure 1) were obtained by cooling various solvent compositions to the temperature at which a large increase in viscosity was noted by the difficulty with which a platinum stirring rod could be moved through the solution. At temperatures below 850°C the viscosity increases rapidly with time, and the data given pertain to times of the order of 10-30 minutes. At longer times (several hours at temperatures below 850°C), the initially fluid compositions often almost completely hardened to a glassy state. Figure 1 thus reflects solvent properties for a dynamic crystal growth situation rather than true phase equilibria of the solvent.

The solvent compositions employed for garnet crystal growth were

A. 47.49% BaF_2†	B. 34.80% BaO	C. 41.00 % BaO
52.51% B_2O_3	34.80% B_2O_3	41.00 % B_2O_3
	30.40% BaF_2	18.00 % BaF_2

*All chemicals are 99.99 wt. % or higher purity.

†All compositions are in mole percent unless otherwise specified.

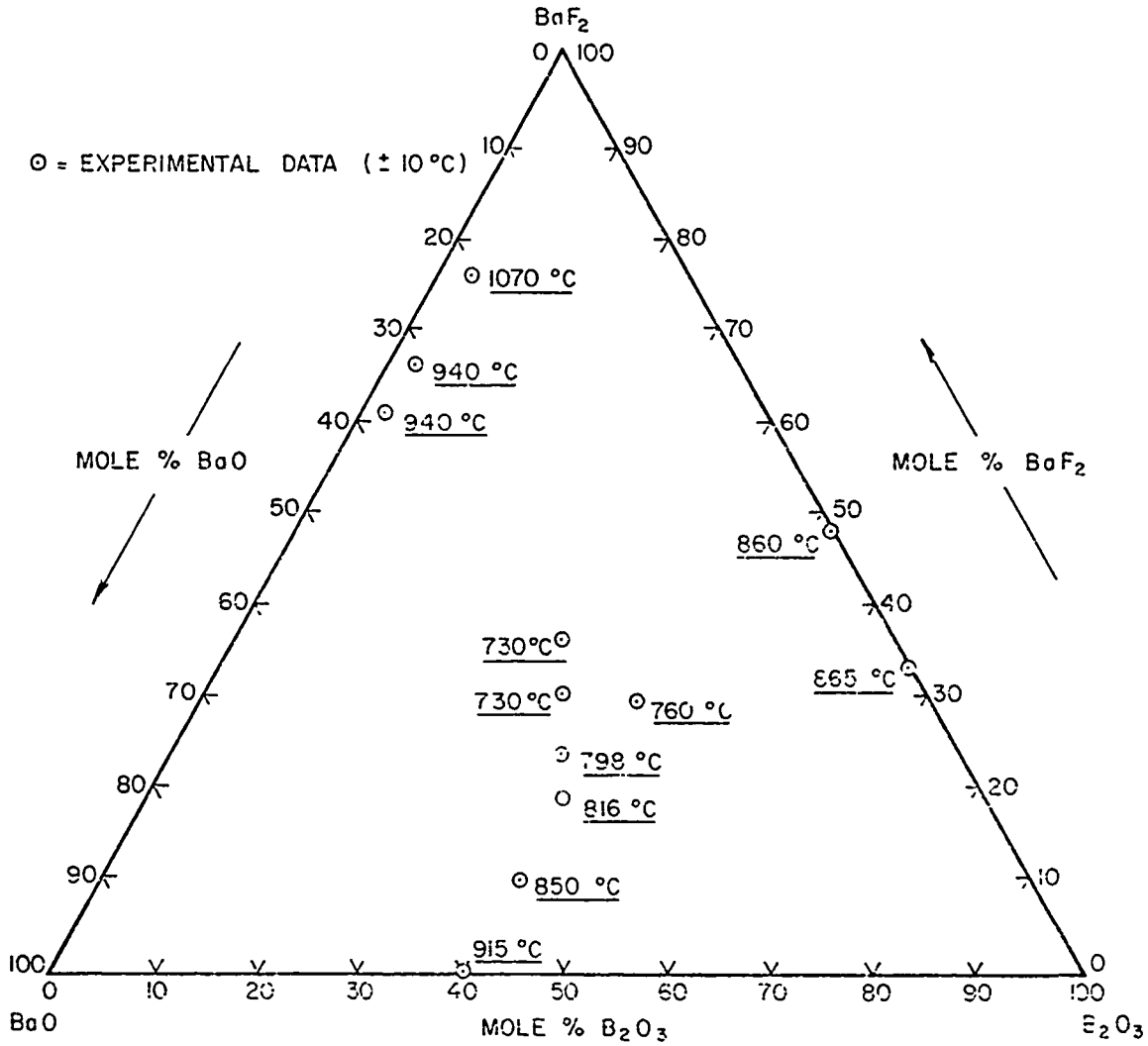

Figure 1. Approximate Liquidus Points for the $BaO-B_2O_3-BaF_2$ System (the points represent approximate temperatures at which a large qualitative increase in viscosity was noted).

The most appropriate of these three compositions (with respect to solvent stability and retention of solution fluidity) was found to be solvent C. The weight loss of this composition was negligible after periods as long as 72 hours at 1450°C. The (nonequilibrium) stability range of the garnet phase in this solution is indicated by the fact that garnet epitaxial layers could be grown at all solute compositions from 7% to 42.5% rare earth oxide content, but compositions on the iron rich side of stoichiometry often produced large quantities of red hexagonal platelets which exhibited an X-ray diffraction pattern similar to barium ferrite and were presumed to be a gallium substituted barium ferrite.

A solubility curve (Figure 2) for $EuEr_2Ga_{0.7}Fe_{4.3}O_{12}$ in solvent C was determined by suspending a polished {111} $Gd_3Ga_5O_{12}$ substrate in a solution containing solute with 42.5% rare earth content, and noting the highest temperature at which an epitaxial layer appeared on the substrate after 20 minutes in the isothermal solution.

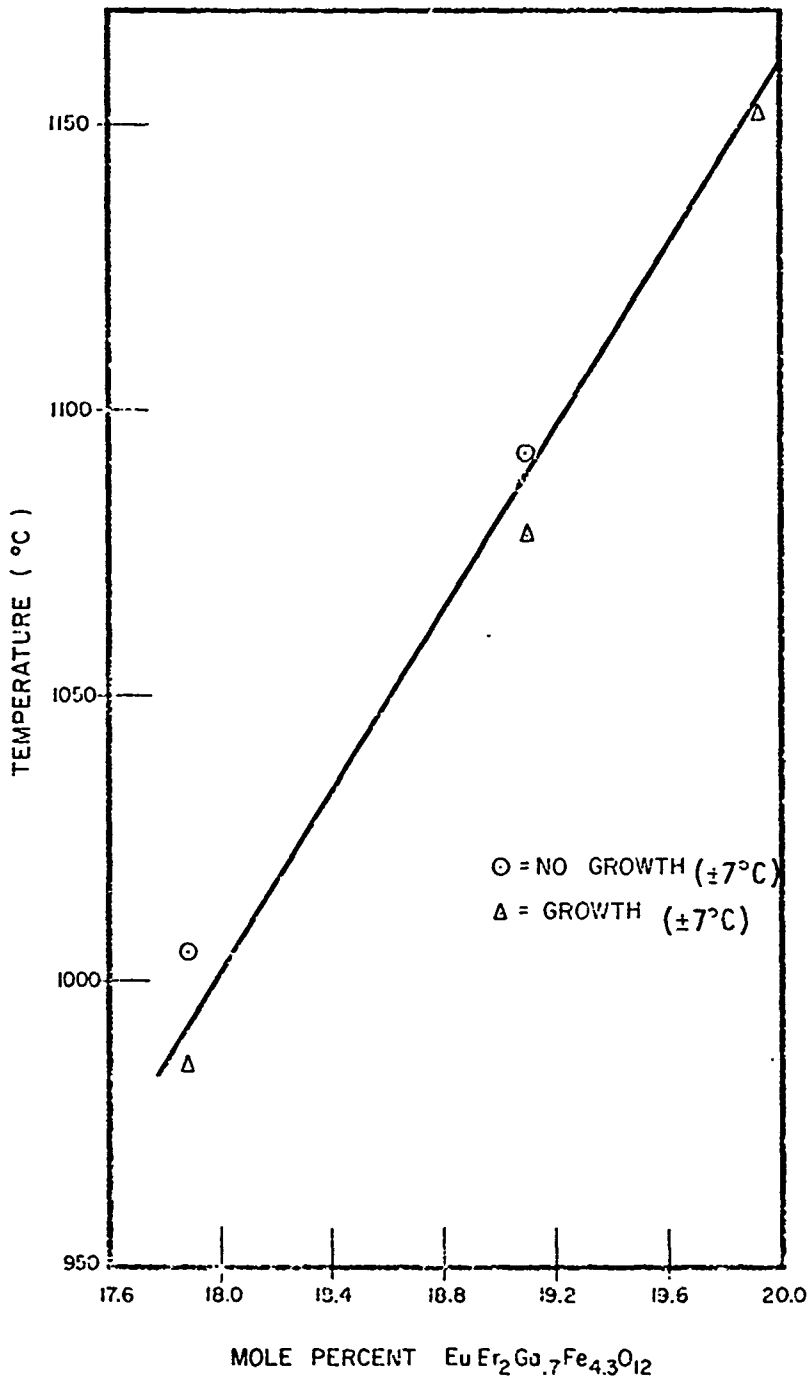

Figure 2. Approximate Solubility Curve for $EuEr_2Ga_{0.7}Fe_{4.3}O_{12}$ in 41 (mole)% BaO, 41% B_2O_3, 18% BaF_2.

2.2.2. Substrate Preparation

2.2.2.1. Boule and Substrate Processing

Substrate material acquired in boule form was sawed into 0.5 mm thick wafers with an annular (I.D.) saw fitted with a diamond impregnated blade. The surfaces of the substrate blanks were first lapped with 3μm alumina to flatten the surface and remove the last trace of saw damage. The amount of material removed in this step depended upon the history of the individual substrate, but was generally 20-30 μm. After lapping, the substrate surface was prepolished with 1μm diamond grit on a nylon pad, and approximately 12μm of material was removed to eliminate all lapping damage. The final 15-25 μm was removed with Syton,* which consists of a colloidal suspension of silica particles (400Å diam.) in a caustic solution.

2.2.2.2. Substrate Characterization and Evaluation

Substrate lattice parameters were measured by the Debye-Scherrer and single crystal X-ray diffractometry techniques described in Reference 5, and were found to be in the range of 12.379-12.384Å. The substrate orientation was determined by Laue X-ray diffraction analysis to be <111> ±1°.

*A product of Monsanto Company

Defects in the substrates, such as dislocations, growth striations, inclusions and the core defect (caused by the formation of {211} facets on the growth interface) were studied by a variety of techniques. Dislocations were detected by optical and X-ray techniques as well as by etch pitting. The stress birfringence resulting from the localized strain surrounding a dislocation is readily observable in transmitted polarized light as shown in Figure 3, and the dislocation lines could thus be tracked through the substrate. These dislocations passed through the substrate at random angles ranging from 45° - 90° to the surface and some appeared to be curved.

Etch pits were generated at the point of intersection of the dislocation with the surface by either 85% orthophosphoric acid at 160°C or a mixture of 50% (by volume) orthophosphoric and 50% sulfuric acid at the same temperature. The mixture acids etched material ~ five times more rapidly than orthophosphoric acid alone. Figure 4 shows the same area on opposite sides of a substrate (0.017" thick), and illustrates the lateral displacement of the dislocations through the substrate. The triangular pits are formed from dislocations less steeply inclined to the surface than those forming the hexagonal pits. These observations combined with the polarized light technique confirmed a 1:1 correspondence between the etch pits and dislocations. Typically, the substrates used for epitaxial growth contained 10-100 dislocations/cm^2. The dislocation etchants also revealed growth striations in substrates cut from boules containing the core defect.[21] The striation spacing was measured with a profilometer and found to be ~ 60 μm.

These phenomena in the substrates were also studied by two X-ray topography techniques. The first, Lang transmission topography, was performed

on substrates thinned to approximately 100 μm, using molybdenum Kα radiation and diffraction from the (220) planes. Photographic plates with G5 emulsion from Ilford Ltd. were used. The second technique utilized scanning reflection topography with copper $K\alpha_1$ radiation, diffracted from the (888) planes, to examine the top surface (to a depth of 5 μm) of the substrates and epitaxial layers.

Typical substrate features are illustrated in Figures 5-7. Figure 5 shows a transmission X-ray topograph of the core defect. (The heavy irregular line running along the upper left hand corner of the topograph is a crack in the substrate.) Similar topographs have been produced in $Y_3Al_5O_{12}$,[22] as well as other magnetic garnet substrate materials.[23] The three lobed strain pattern observed by stress birefringence can also be seen in this topograph. In agreement with the findings of Basterfield et al.,[22] the crystallographic directions of the axes of the lobes are (211), (121) and (112) as determined by comparing the topograph with a Laue diffraction pattern. The striation spacing varied from 38 μm near the periphery to 75 μm at the center of the substrate, in agreement with the etching studies.

Figure 6 shows a scanning reflection topograph of an epitaxial layer of $Gd_{0.79}Y_{1.46}Yb_{0.75}Fe_{4.1}Ga_{0.9}O_{12}$ (2.8 μm thick) grown on a substrate containing a core defect, which illustrates the reproduction of the strain from the substrate core in the epitaxial growth. Figure 7 illustrates the striation pattern in a core free substrate. The magnitude of the lattice parameter variation causing these striations is not known but is probably $\leq \pm 0.001$Å, and the effect upon magnetic properties of the epitaxial films has not been quantitatively determined.

Reproduced from best available copy.

Figure 3. Strain fields caused by dislocations in $Gd_3Ga_5O_{12}$ substrate. (Transmitted polarized light, 200X.)

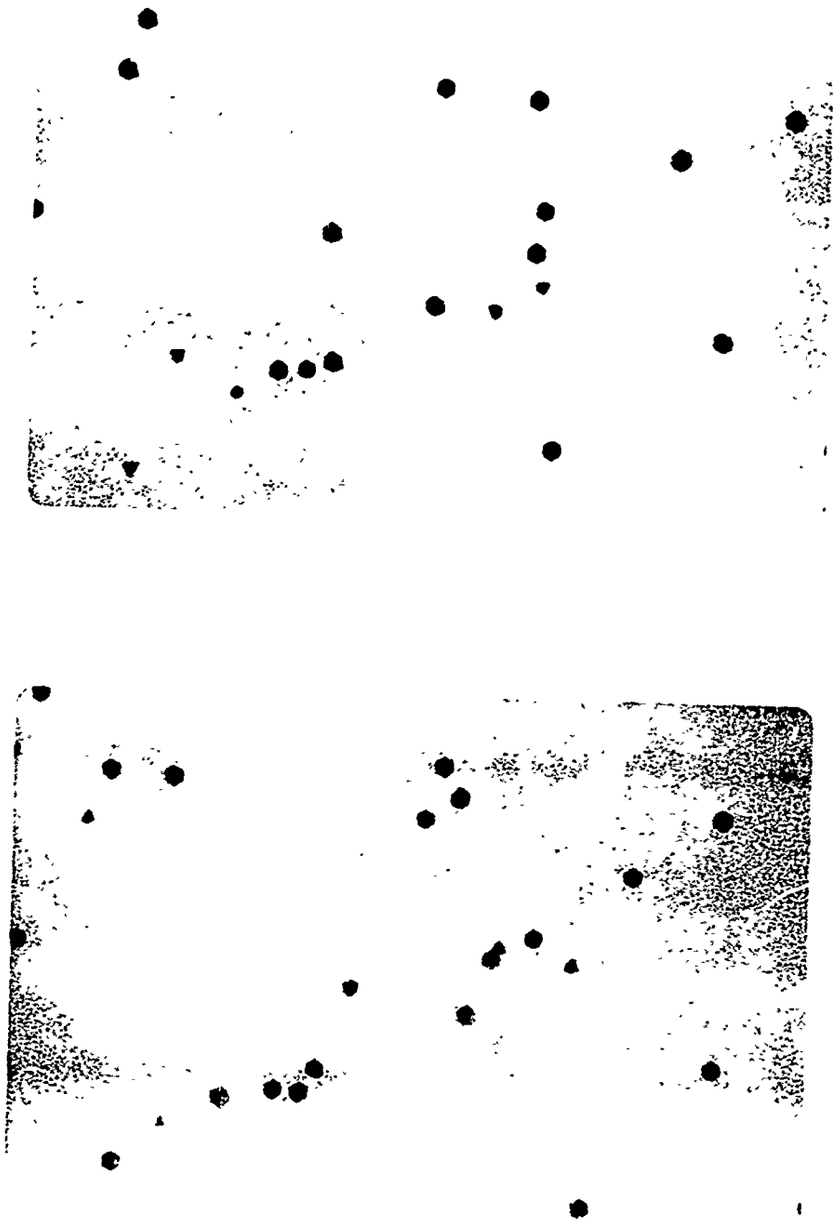

Figure 4. Dislocation etch pits in a <111> $Gd_3Ga_5O_{12}$ substrate. Upper photo is of top surface of substrate, lower photo is the same area on the bottom surface. (200X)

Reproduced from best available copy.

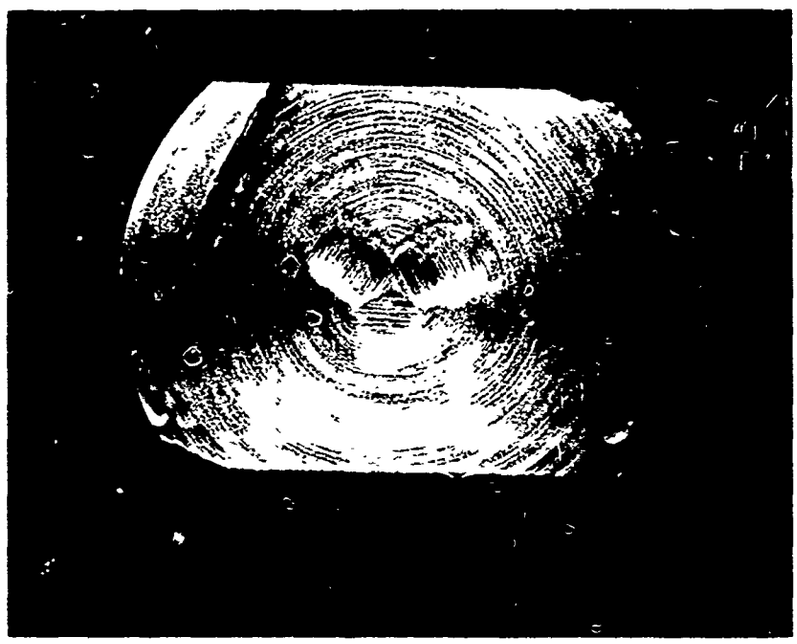

Figure 5. Lang transmission topograph of a thin (110μm) <111> $Gd_3Ga_5O_{12}$ substrate containing a "core" defect. (220) reflection, MoKα radiation, 5.3X.

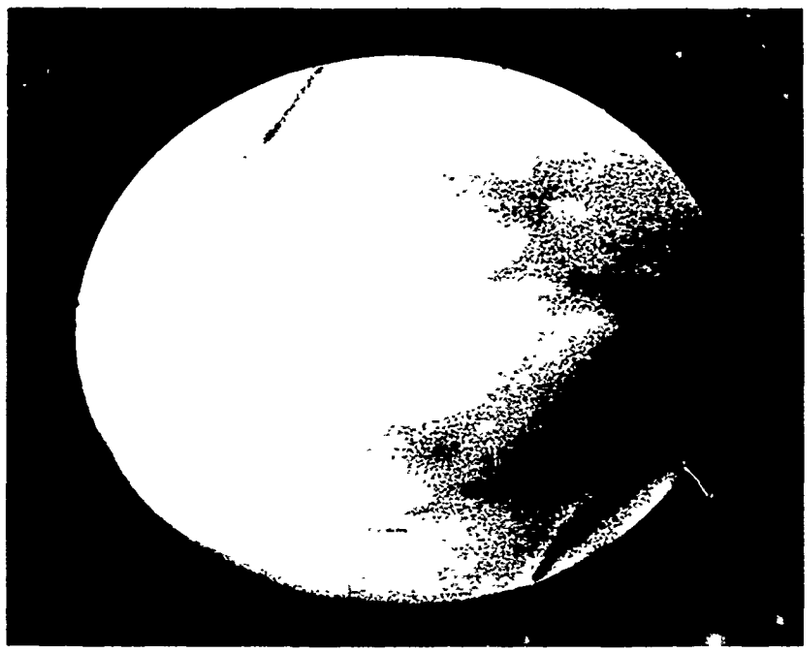

Figure 6. Scanning reflection topograph of an epitaxial film of $Gd_{0.79}Y_{1.46}Yb_{0.75}Fe_{4.1}Ga_{0.9}O_{12}$ grown on a cored substrate. (888) reflection, $CuK\alpha$ radiation, 6X.

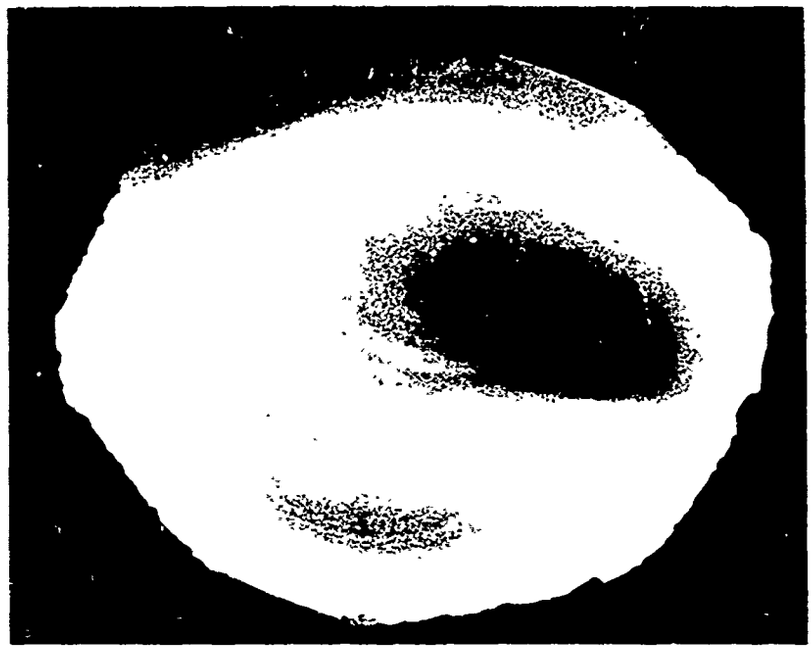

Figure 7. Scanning reflection topograph of a core free, dislocation free <111> $Gd_3Ga_5O_{12}$ substrate. (888) reflection, CuKα radiation, 6X .

2.2.3. Crystal Growth

The growth of the $(Eu,Er)_3\ (Ga,Fe)_5O_{12}$ garnets has been described in previous reports,[4,5] and the discussion here will center on the growth of the $(Gd,Y,Yb)_3\ (Ga,Fe)_5O_{12}$ compositions in both BaO-based and PbO-based solvents, since the growth technique does not basically change for variations in garnet composition.

2.2.3.1. Growth in BaO-based Solvents

The solvent composition employed was 41% BaO, 41% B_2O_3 and 18% BaF_2. The 19% solute concentration in this solution was comprised of 42.4% rare earth oxides and 57.6% metal oxides. The solute composition consisted of $Gd_xY_{2.25-x}Yb_{0.75}Ga_{0.9}Fe_{4.1}O_{12}$ where x ranged from 0.7 to 0.98. A typical composition is as follows: $BaCO_3$ 95.25 gm, B_2O_3 33.61 gm, BaF_2 37.15 gm, Fe_2O_3 20.98 gm, Ga_2O_3 5.41 gm, Gd_2O_3 12.23 gm, Y_2O_3 12.02 gm, Yb_2O_3 11.42 gm. This mixture was placed in a 100 cc platinum crucible, thermal decomposition and initial melting were carried out at 1000-1100°C, and then the charge was placed into the growth furnace, which maintained the solution in an isothermal (±0.5°C) condition.

In all cases, the dipping technique of LPE growth was used with the substrate held vertically in a quiescent solution as shown in Figure 8. Several types of substrate holders were employed, but in all cases the substrates were polished and layers were grown on both sides.

Before each growth run, the solution was heated to 1250°C and stirred to ensure complete dissolution of all constituents. The equilibration time required at 1250°C did not seem critical, and the solution was routinely kept

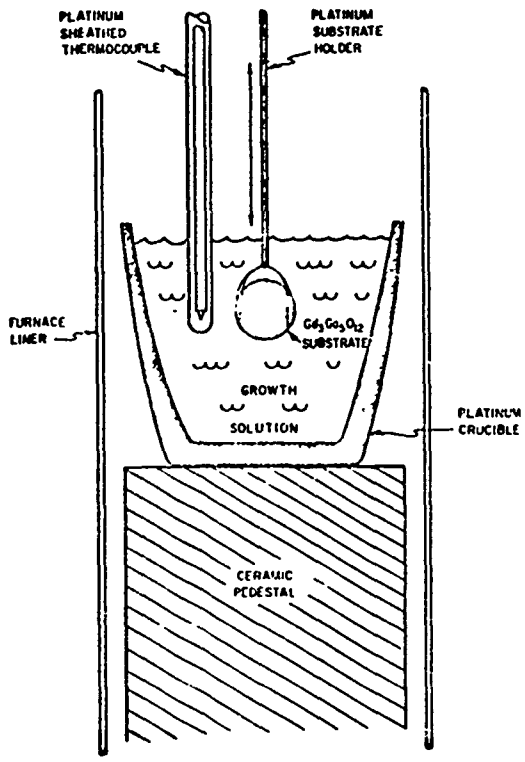

Figure 8. Apparatus for Epitaxial Crystal Growth of Magnetic Bubble Garnets.

at this temperature between growth runs. The growth runs consisted primarily of either (i) a cooling run from 1040°C-990°C at ~ 2-3°C/min. or (ii) an isothermal growth run at 990°C. In either case, the solution was stirred at 1100°C as it cooled down and then left undisturbed for the duration of the run. The substrate was equilibrated at the same temperature as the solution for 2-5 minutes before insertion.

The critical step in LPE growth from the BaO-based solution is the removal of the solution from the epitaxial layer after growth. The solution is too viscous and wets the garnet too well to be drained off by gravitational forces at growth temperatures < 1050°C, and the film which remains on the epitaxial layer is strong enough to crack and spall the layer as they cool to room temperature, due to the difference in thermal expansion. The solution can be removed, however, by a very slow and uniform withdrawal of the layer from the solution at rates as low as 0.15"/min. At this rate, the surface tension of the solution is high enough to keep the surface intact as the layer is withdrawn, effectively wiping the layer clean of solution.

2.2.3.1.1. Results and Discussion of Growth in BaO-Based Solvents

The growth parameters for typical LPE growth runs of $Gd_xY_{2.25-x}Yb_{0.75}Ga_{0.9}Fe_{4.1}O_{12}$ are shown in Table III. All growth occurred in the solution composition described in Section 2.2.3.1., which appears to be adequate for LPE growth.

A series of growth runs at 990°C for various lengths of time indicated that the initial growth rate of the epitaxial film is very nonlinear up to

TABLE III

Growth Parameters for LPE Garnet Growth in $BaO-B_2O_3-BaF_2$ Solvent

Run No.	x in $Gd_xY_{2.25-x}Yb_{0.75}Ga_{0.9}Fe_{4.1}O_{12}$*	Equilibration Time at 1250°C (hr)	Run Temp. (°C) (±1°C)	Run Time or Cooling Rate (±0.1°/min)	Thickness (μm) (±0.3μm)	Lattice Parameter(Å)+ (±0.001Å)	Remarks
LS68	0.7	16	1040→990	1.66°C/min	2.1	12.370	Specular, stripe domains
LS95	0.98	16	1040→990	1.72°C/min	3	12.391	Faceted, no domains
LS102	0.873	39	990	9 min	3	12.381	Specular, large irregular domains
LS112	0.845	18	990	5 min	1.7	12.381	Specular, stripe domains
LS120	0.7	2.25	1040→990	2.3°C/min	3.6	12.370	Specular, stripe domains
LS121	0.7	38	1040→990	2.3°C/min	3.5	12.370	Specular, stripe domains
LS122	0.7	2.25	1040→990	2.3°C/min	3.8	12.370	Specular, stripe domains

*Solution Composition

+Standardized to a substrate lattice parameter a_o = 12.382Å.

about 2.6μm, as shown in Figure 9. After this initial transient, the growth appears to be steady state and much slower. The initial rapid growth may be caused by nonuniform depletion of ions in the boundary layer adjacent to the interface, followed by a steady state diffusion through the boundary layer to the growth interface, where the most slowly diffusing ion determines the rate limiting step. Differences in ionic diffusion coefficients of the various crystal constituents or an initial meltback of the substrate before growth begins may lead to composition variations normal to the interface, and some evidence of this will be presented in Section 3.9.

The layers with lattice parameters considerably less than that of the substrate ($a_{sub.} - a_{epi} > 0.005\mathring{A}$) were specular while those with lattice parameters very close to the substrate ($a_{sub.} - a_{epi} < \pm 0.002\mathring{A}$) were sometimes slightly roughened with a peak-to-valley distance < 1μm. Films with lattice parameters considerably greater than the substrate ($a_{epi} - a_{sub} > 0.005\mathring{A}$), were usually faceted, and often did not exhibit stripe or bubble domains.

Aside from the cracking and spalling seen in early films, the only defects observed in the films were ~ 5 - 10 μm triangular pits which appeared to originate from substrate dislocations or particulate matter on the substrate surface on the basis of qualitative observations of the defect density and distribution in the films and substrates. A defect density figure in terms of defects/cm^2 is not very meaningful for these films. Magnetic bubble devices require defect free areas on the film > 10 mm^2, and the best layers had areas of 10-20 mm^2 which were defect free.

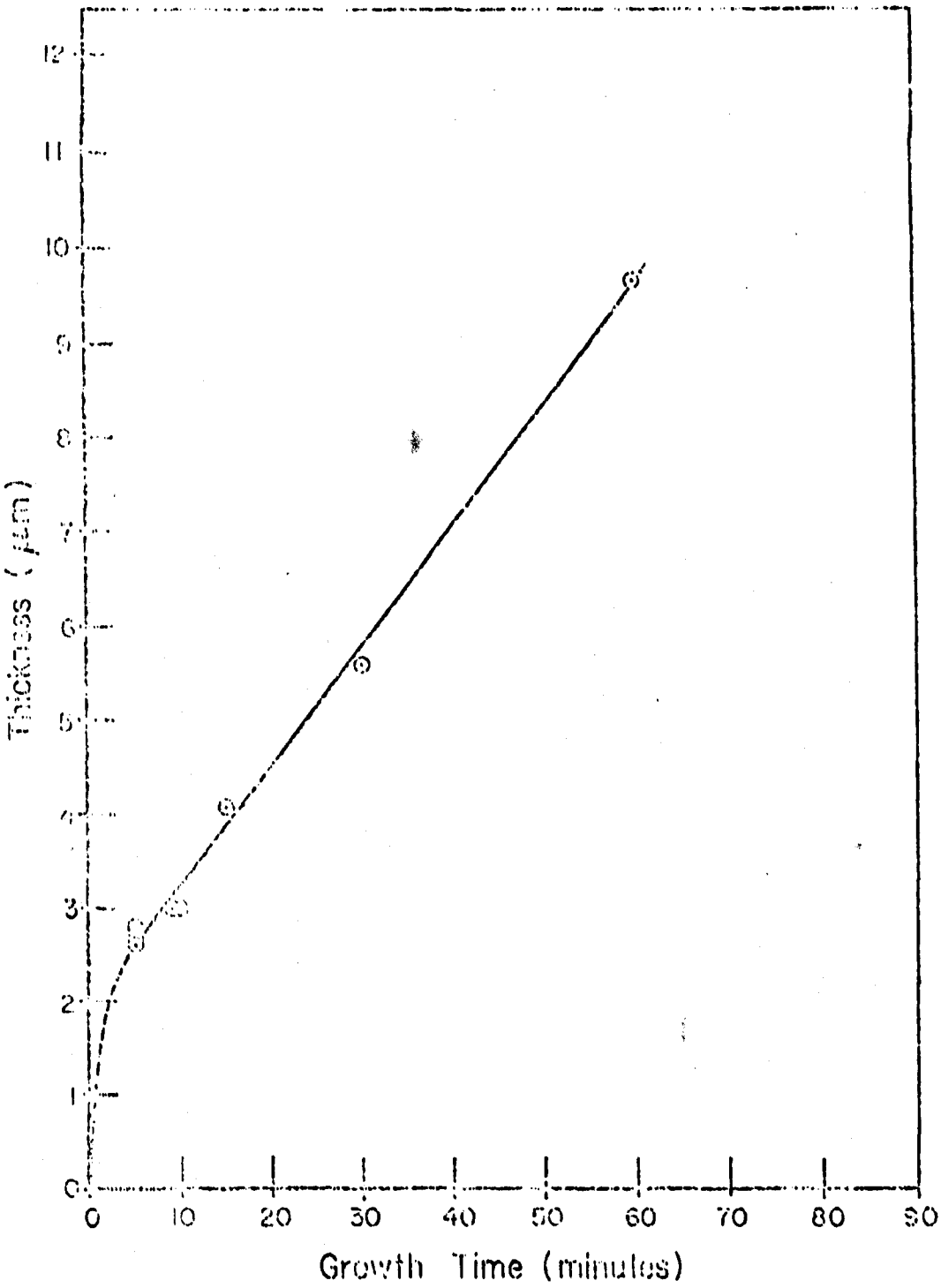

Figure 9. Growth rate of $Gd_{0.7}Y_{1.55}Yb_{0.75}Ga_{0.9}Fe_{4.1}O_{12}$ at 990°C in $BaO-B_2O_3-BaF_2$ solvent.

2.2.3.2. Results of Growth in PbO-based Solvents

A series of growth runs in a $PbO-B_2O_3$ solvent was carried out for comparison with the epitaxial layers grown in the BaO-based solvents. Magnetic films of $(Eu,Er)_3\ (Fe,Ga)_5O_{12}$ and $(Gd,Y,Yb)_3\ (Fe,Ga)_5O_{12}$ were grown on {111} $Gd_3Ga_5O_{12}$ substrates by the dipping technique at temperatures ranging from 850 to 943°C. Most of the runs were performed at an isothermal growth temperature, while a few were carried out by rapid cooling techniques from 900-850°C.[5] In all cases, the solvent contained 93.7% PbO and 6.3% B_2O_3. The solute concentration was varied from 6.66% to 13.11%, and the rare earth concentration in the solute ranged from 20.23 to 10.13%.

Although epitaxial garnet layers could be grown from all these compositions, red orthoferrite platelets were also present on the epitaxial layer for all rare earth concentrations except the 10.13%. This value is not in agreement with a recently reported phase diagram,[24] but it does appear to be in the garnet phase field under these crystal growth conditions. In addition to these second-phase defects, triangular pits were often seen in the epitaxial layer, which trapped solution as the substrate was pulled out of the solvent after growth. Continuing growth under this region of trapped solution produced steps in the epitaxial layer. The defects were attributed to substrate dislocations and foreign particles on the substrate surface before growth, again on the basis of the qualitative observation of the defect density and distribution in the substrates and films.

Growth parameters of typical runs at 900°C are given in Table IV. The initial transient appears to be much less evident in this solvent as indicated by the data shown in Figure 10, which may be caused by thermal convection in the solution during growth. The steady state growth rate is almost 3 times greater than in the BaO-based solvent, even though the initial supercooling is not as large. This may be attributed to the flatter garnet liquidus slope in the $PbO-B_2O_3$ solvent (resulting in greater supersaturation for a given amount of supercooling) as well as the possibility of more rapid growth kinetics in the $PbO-B_2O_3$ solvent. A comparison of some of the properties of epitaxial layers grown in the PbO-based solvent with those grown in the BaO-based solvent will be discussed in Section III.

TABLE IV

Growth Parameters for $(Gd,Y,Yb)_3(Ga,Fe)_5O_{12}$ Grown in $PbO-B_2O_3$ Solvent

Run No.	Solution Composition	Equilibration Temp./Time	Run Temp. (±0.3°C) Run Time (±0.1 min)	Thickness (μm) (±0.3 μm)	Lattice* Parameter (Å) (±0.001Å)
FP46	$Gd_{.785}Y_{1.465}Yb_{.75}Ga_{.6}Fe_{4.4}O_{12}$	1075°C 1 hr	900°C 7.5 min.	2.1	12.375
FP51	$Gd_{.785}Y_{1.465}Yb_{.75}Ga_{.36}Fe_{4.64}O_{12}$	1050°C 3 hrs.	900°C 12 min.	3.7	12.379
FP57	$Gd_{.7}Y_{1.55}Yb_{.75}Ga_{.4}Fe_{4.6}O_{12}$	1070°C 1 hr	900°C 9 min.	2.8	12.381
FP59	$Gd_{.7}Y_{1.55}Yb_{.75}Ga_{.4}Fe_{4.6}O_{12}$	1052°C 1 hr	900°C 10.75 min.	3.0	12.379
FP62	$Gd_{.7}Y_{1.55}Yb_{.75}Ga_{.46}Fe_{4.54}O_{12}$	1058°C 1 hr	900°C 15 min.	4.5	12.380

* Standardized to a substrate lattice parameter a_o = 12.382Å.

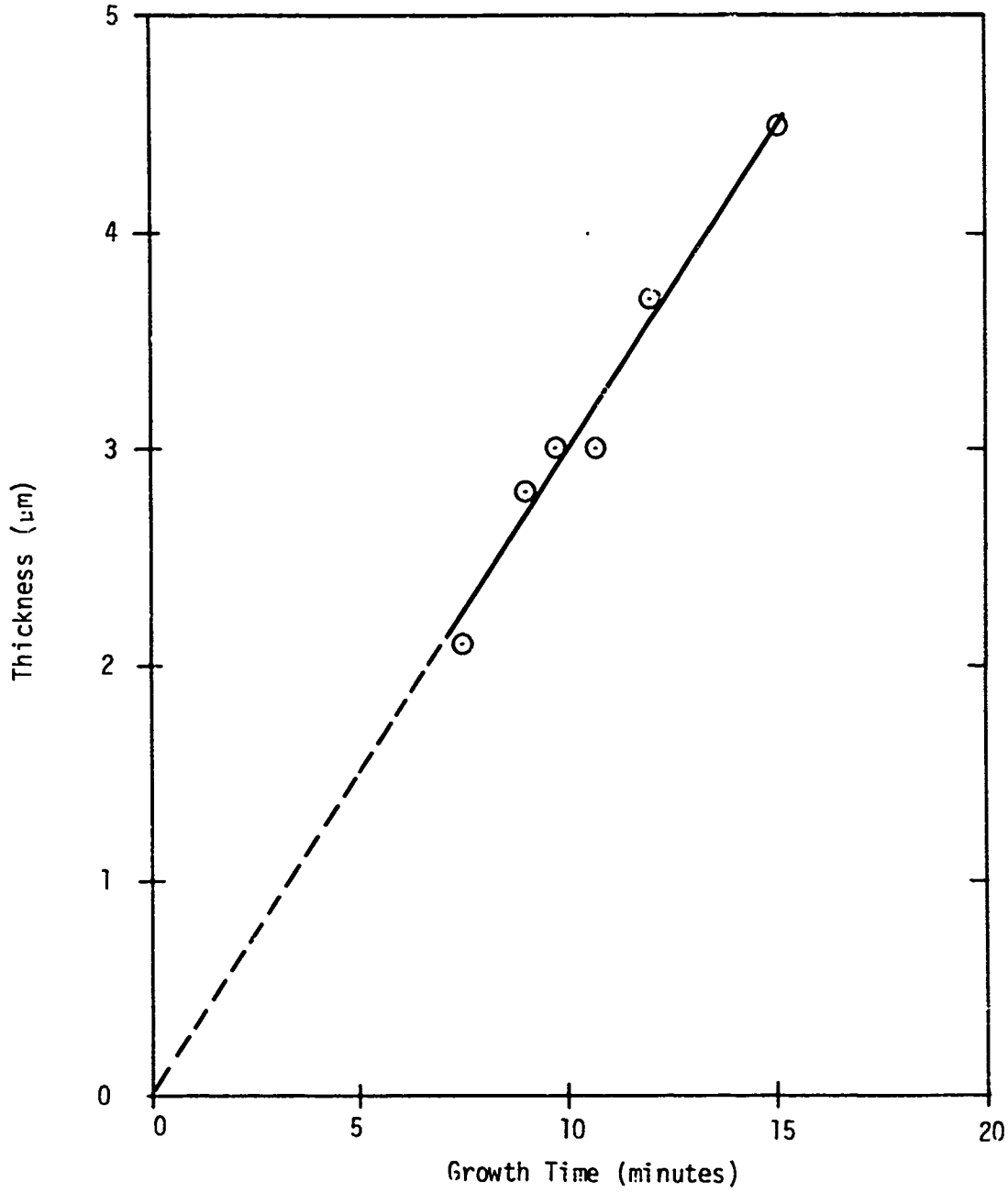

Figure 10. Growth Rate of $(Gd,Y,Yb)_3\ (Fe,Ga)_5O_{12}$ at 900°C in $PbO-B_2O_3$ Solvent.

SECTION III

3.0. CHARACTERIZATION AND EVALUATION

Film characterization and evaluation formed a major portion of the effort during the latter phase of this contract period, aided substantially by a separate company-sponsored program. The epitaxial layers were characterized with respect to the parameters shown in Table V. The impurity and compositional analyses were performed primarily on the $(Eu,Er)_3(Ga,Fe)_5O_{12}$ compositions grown during the first phase of this contract period and the remainder of the characterization was performed on $(Gd,Y,Yb)_3(Ga,Fe)_5O_{12}$ compositions.

3.1. Film Surface Morphology and Magnetic Defect Density

Defects in films grown in the BaO-based solvent appeared to be of two types; (i) catastrophic cracking and spalling caused by the difference in thermal expansion between garnet and adhered solution as they cooled down to room temperature, and (ii) defects such as pits related to substrate dislocations and particulate matter lying on or embedded in the substrate surface.

An example of catastrophic cracking and spalling can be seen in Figure 11a. Figure 11b shows that this type of defect can be effectively eliminated by appropriate processing techniques as discussed in Section 2.2.3.1, and this is no longer considered to be a problem in the use of the BaO-based solvent. The PbO-based solution readily runs off the surface after growth as shown by the as-grown epitaxial layer in Figure 12.

TABLE V

Characterization Techniques for Magnetic Rare Earth Garnets

Parameter	Current HPL Method	Alternative Method
1. Substrate and film surface perfection	Etch pit studies, Berg-Barrett and Lang topography, optical microscopic mapping, scanning electron microscopy	
2. Impurity analysis	Emission spectroscopy, microprobe analysis	Atomic fluorescence, wet chemistry
3. Film composition and compositional homogeneity	Microprobe, lattice parameter measurement, calculate from magnetization and Neél temperature	Atomic fluorescence
4. Film-substrate lattice parameter difference and film lattice parameter	X-ray diffractometry	
5. Film thickness and thickness uniformity	Metallographic cross section, interferometry	Profilometry, infrared interference
6. Magnetization	Static collapse of bubbles, Torque magnetometer, Stripe domain width	Vibrating sample magnetometer
7. Characteristic length	Bubble collapse diameter, Stripe domain width	
8. Wall energy	Calculate from $\sigma_w = 4\pi M^2 \ell$	Sinusoidal wall technique
9. Anisotropy constants	Torque magnetometer	[illegible]-plane field with Faraday effect
10. Mobility	Pulse optical modulation, Dynamic bubble collapse	
11. Coercive force	AC optical modulation	Stable bubble separation, magnetic gradient technique
12. Neél Temperature	Faraday effect domain observation in hot stage microscope	Microbalance susceptibility measurement
13. Stripe width temperature coefficient	Faraday effect domain observation in hot stage microscope	Faraday effect in cryogenic environment
14. Index of refraction	Brewster angle	Reflection intensity

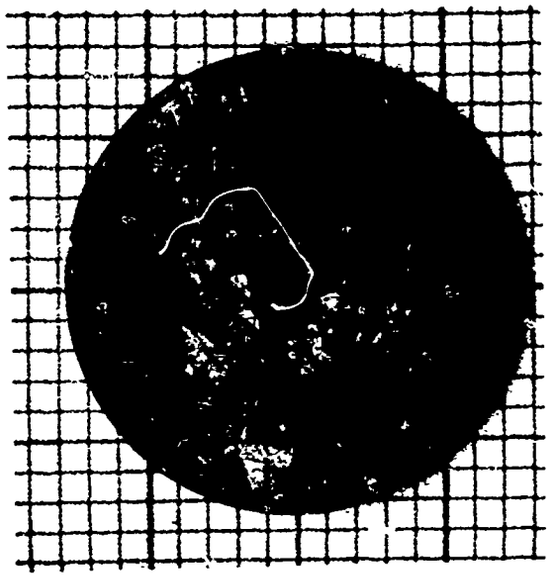

Figure 11a. Surface Morphology of $Gd_{0.7}Y_{1.55}Yb_{0.75}Ga_{0.9}Fe_{4.1}O_{12}$ grown on $Gd_3Ga_5O_{12}$ in $BaO-B_2O_3-BaF_2$ solvent after adhered solution has been etched off.

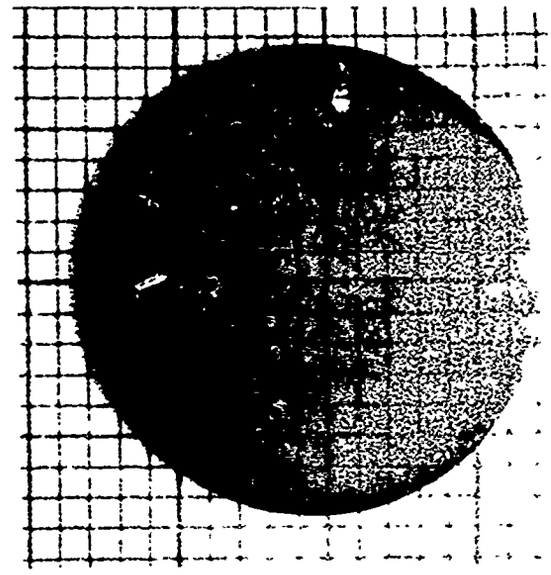

Figure 11b. Surface Morphology of $Gd_{0.7}Y_{1.55}Yb_{0.75}Ga_{0.9}Fe_{4.1}O_{12}$ grown on $Gd_3Ga_5O_{12}$ in $BaO-B_2O_3-BaF_2$ solvent with slow withdrawal from solution.

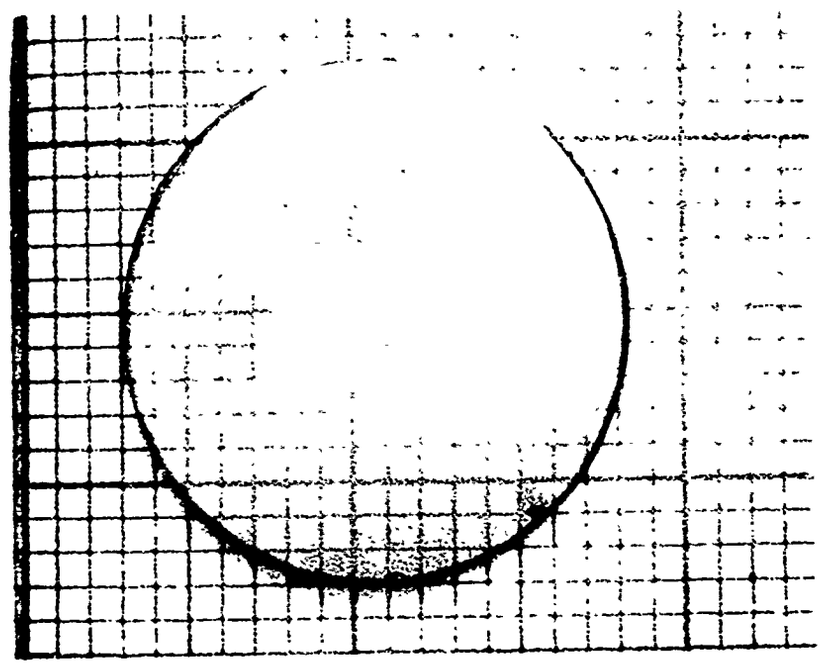

Figure 12. As grown $Gd_{0.7}Y_{1.55}Yb_{0.75}Ga_{0.9}Fe_{4.1}O_{12}$ epitaxial film grown on $Gd_3Ga_5O_{12}$ from a $PbO-B_2O_3$ growth solution.

Most of the localized substrate defects can be eliminated by proper substrate growth and processing techniques. The highest quality layer to date has been grown in the $PbO-B_2O_3$ solvent, and has 29 pits in the central one cm^2 area of the layer with the largest defect free area > 30 mm^2.

The nonlocalized surface morphology of the epitaxial layers varies, depending upon substrate homogeneity and processing techniques. In some cases, particularly for films grown in compression, the morphology has been rough and faceted. This problem has, however, been eliminated by proper choice of composition and growth parameters, and films grown by suitable techniques exhibit completely specular and featureless surfaces over the entire area of the film in both the PbO-based and BaO-based solvent (except for the localized substrate related defects).

3.2. Film Composition and Impurity Analyses

A detailed specification of composition, although desirable, is difficult because of the large number of cations in the lattice, the small volume of the epitaxial film, and the large effect that the growth parameters have both upon the average crystal composition and the spatial variation within a layer, particularly in the $PbO-B_2O_3$ solvent. Techniques that can be used to give a measure of the chemical composition include emission spectrographic analysis, microprobe analysis, lattice parameter measurements, and the magnetic quantities such as magnetization, characteristic length and Neél temperature. Although we have employed these techniques, in this report we also specify the solution composition and growth parameters of the films, which can be specified more exactly and are more useful for the reproduction of compositions having the properties described.

Emission spectrographic and electron microprobe analyses were performed on garnet epitaxial layers to determine the amount of solvent incorporated into the garnet structure during growth as well as the average composition of the epitaxial films.[5] Distribution coefficients for Ga in octahedral and tetrahedral sites (α_{Ga}), and Eu in dodecahedral sites (α_{Eu}) were derived from the microprobe data by treating the Eu + Er and Ga + Fe as separate entities. These distribution coefficients are complex functions of temperature, growth rate, boundary layer thickness and initial gallium concentration in the solution. α_{Eu} is nearly unity for a wide variety of growth conditions in both PbO-based and BaO-based solvents.

α_{Ga} is nearly unity in the BaO-based solvents and varies little with temperature, while it ranges from 1.5 to 2.3 in the $PbO-B_2O_3$ solvent, depending upon growth parameters. This material parameter is thus much easier to control in the $BaO-B_2O_3-BaF_2$ solvent than in PbO-based solvents.

The variation of lead incorporation with growth rate is shown in Figure 13. This effect (also noted by Giess et al.[12]) is probably caused by a combination of an increase in the lead distribution coefficient and an increase in the amount of micro-inclusions of solvent (<1μm) with growth rate, since these effects are indistinguishable by electron microprobe analysis. The relation between lead or barium incorporation and growth temperature is shown in Figure 14, in which it is assumed that the solvus curve for either lead or barium in the garnet is of the standard form $x = x_0 e^{-\Delta H/RT}$ where x_0 and ΔH are constants over the temperature range of interest. Figure 14 suggests that barium is less soluble in the garnet than lead in the temperature range 850-1050°C, a reasonable result since the Ba^{2+} ion is much larger than the Pb^{2+} ion and also larger than any other cation present in the garnet,[25,26] and therefore may be more difficult to introduce into the lattice.

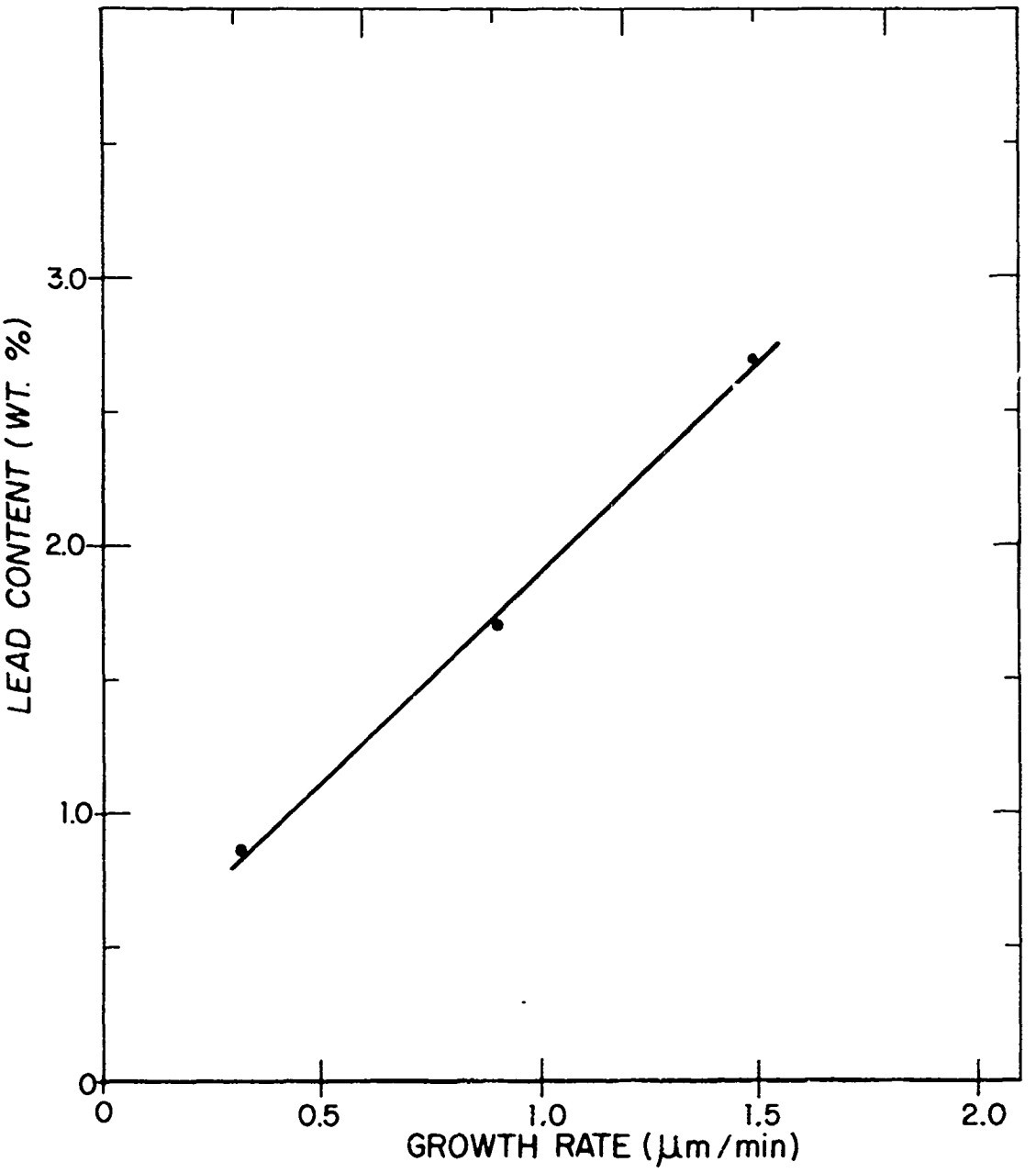

Figure 13. The Growth Rate Dependence of Lead Content in $(Eu,Er)_3(Ga,Fe)_5O_{12}$ Epitaxial Layers Grown by the Cooling Technique from 900 to 850°C.

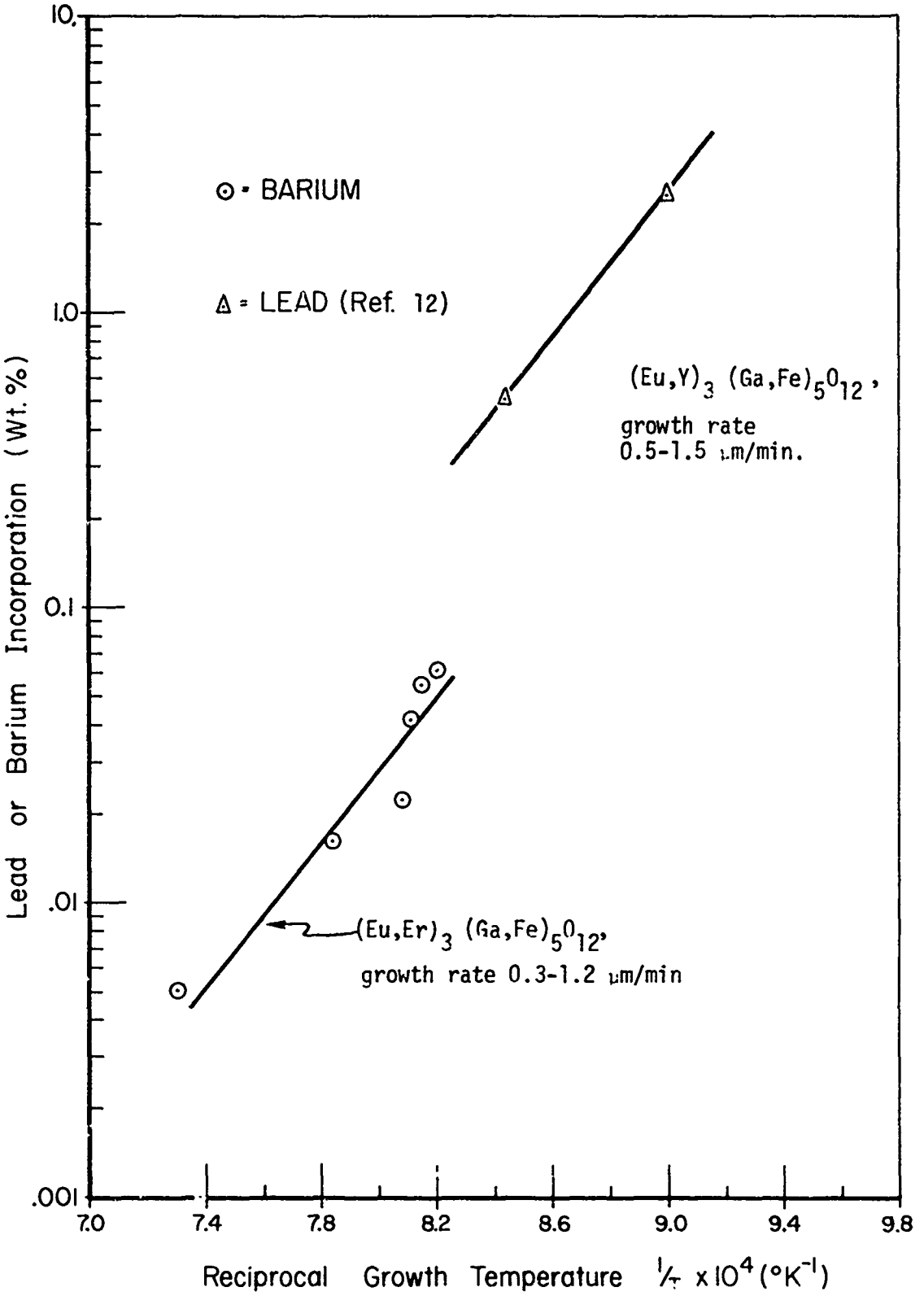

Figure 14. Concentration of lead and barium incorporated in $(Eu,Er)_3\ (Ga,Fe)_5O_{12}$ and $(Eu,Y)_3\ (Fe,Ga)_5O_{12}$ during LPE growth.

3.3. Lattice Parameter Determination

In order to determine the amount of lattice parameter mismatch between epitaxial layers and substrates, the lattice parameters have been measured on a number of samples by either powder pattern or single crystal techniques. The techniques used were described in Reference 5, and the results are summarized here.†

The variation of the lattice parameter of the epitaxial layer with the solution composition $Gd_xY_{2.25-x}Yb_{0.75}Ga_{0.9}Fe_{4.1}O_{12}$ for films grown in the BaO-based solvent at temperatures ranging from 1040°C to 900°C is shown in Figure 15. The numbers in parentheses indicate the number of films grown at each composition (all the lattice parameters measured lie within the ±0.001Å deviation shown). The results indicate an increase in lattice parameter of 0.07Å for each formula unit of Gd added to the solution composition. The lattice parameter does not seem to vary significantly with growth temperature or growth rate since growth data for different temperatures fit the line very well, indicating that the distribution coefficients of Gd^{3+} and Y^{3+} in this range of garnet compositions do not vary significantly with temperature.

The variation of lattice parameter with solution Ga content for two different garnets grown at 900°C in the $PbO-B_2O_3$ solvent is shown in Figure 16. Since the distribution coefficient of Ga varies significantly with temperature in this solvent,[5,12] the growth temperature was kept to 900 ±0.3°C for this series of runs. The results indicate that the rate of decrease in lattice parameter with gallium content varies depending upon the rare earth distribution, and in this case varies from 0.03Å per formula

†All the lattice parameter data are given for the direction normal to the substrate interface. The lattice parameter parallel to the interface may differ depending upon the amount of strain which is induced by the lattice mismatch. The film lattice parameter is normalized in all cases to a substrate lattice parameter a_0 = 12.382A.

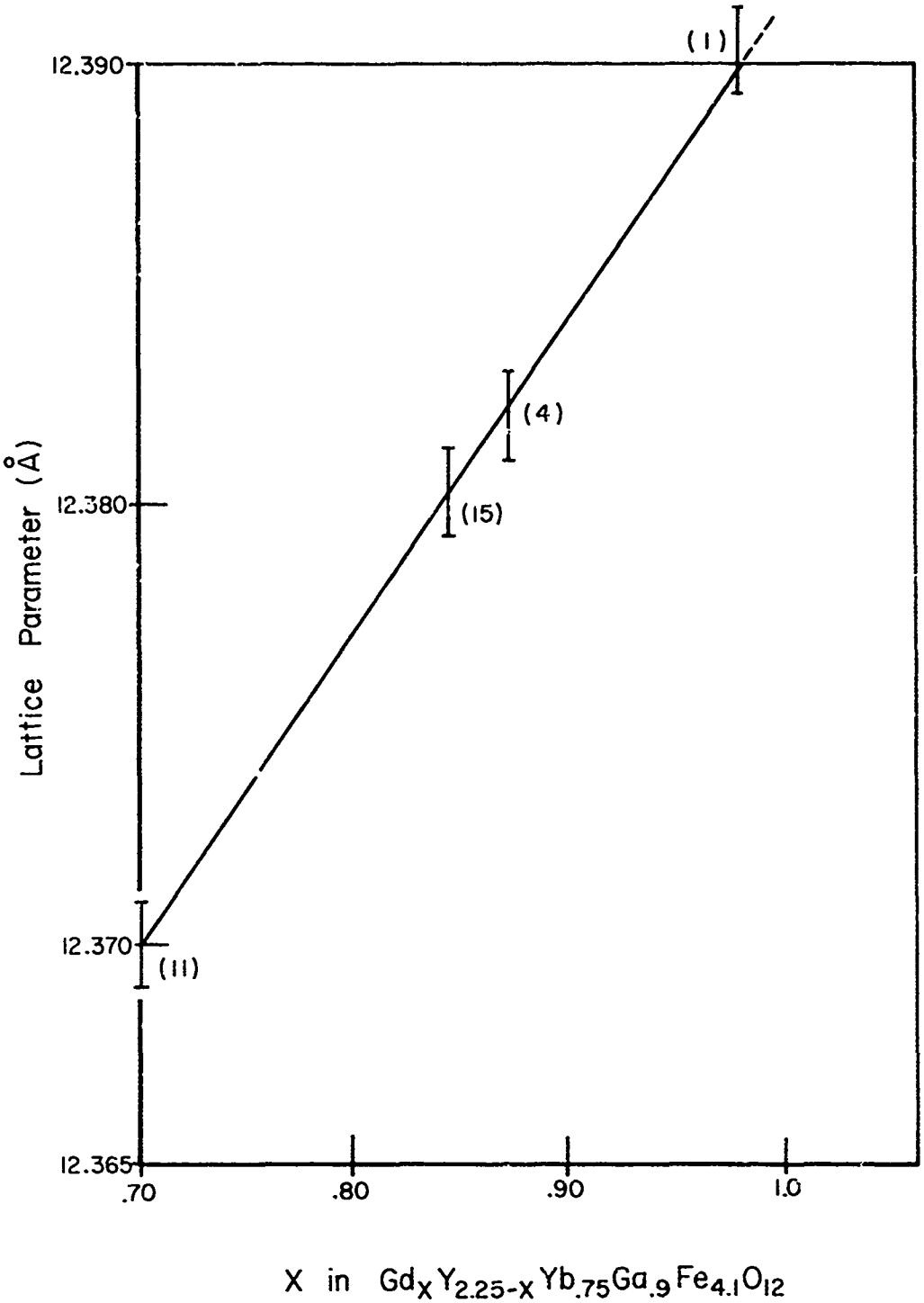

Figure 15. Variation of Lattice Parameter with Solution Composition for Garnet Films Grown in $BaO-BaF_2-B_2O_3$ solvent in the Temperature Range 900-1040°C.

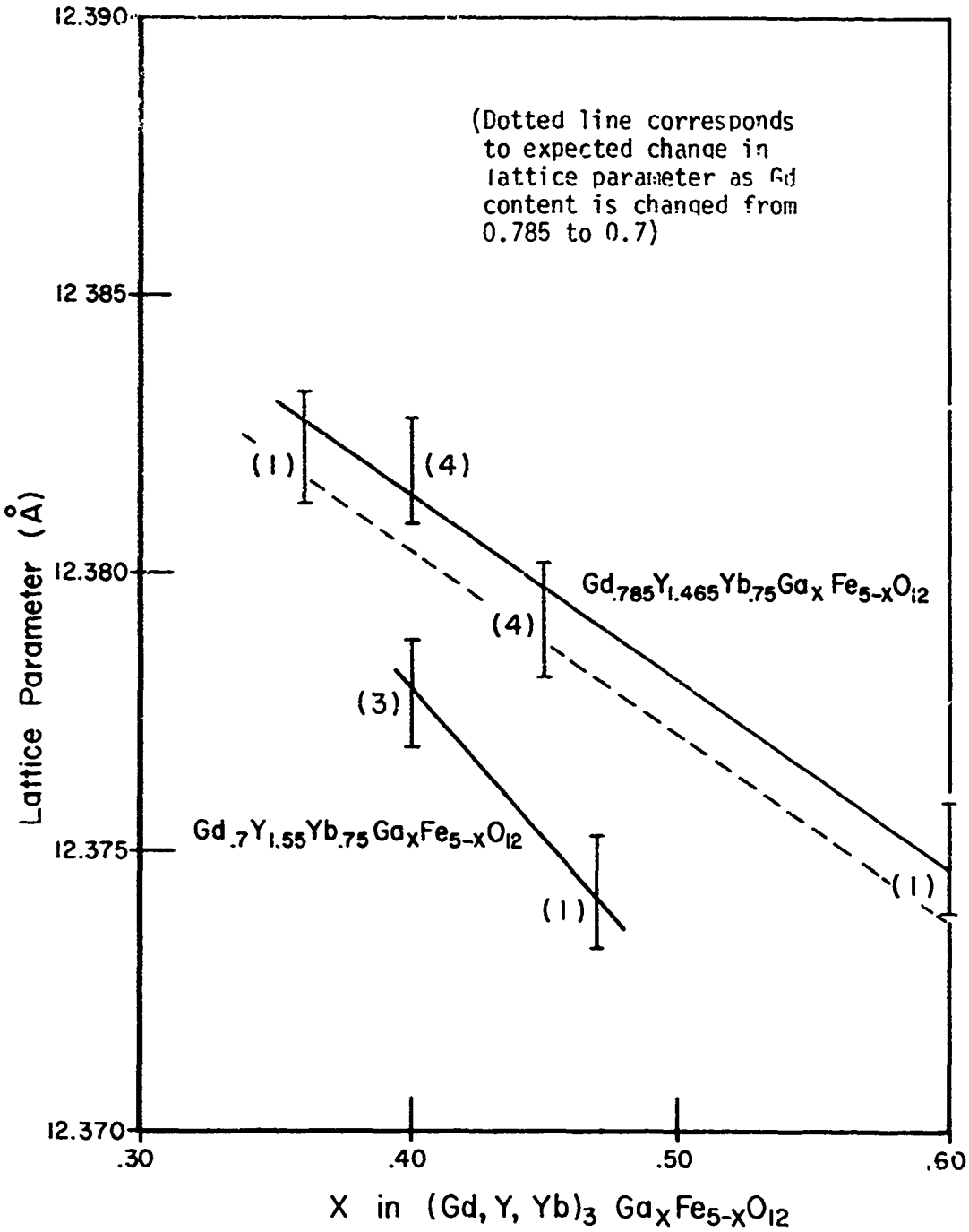

Figure 16. Variation of Lattice Parameter with Solution Gallium Content for Films Grown in $PbO-B_2O_3$ Solvent at 900°C.

unit for $Gd_{0.785}Y_{1.465}Yb_{0.75}Ga_xFe_{5-x}O_{12}$ to 0.055Å per formula unit for $Gd_{0.7}Y_{1.55}Yb_{0.75}Ga_xFe_{5-x}O_{12}$. These results also indicate that the Ga distribution coefficient itself is a function of rare earth content, since if the results of Figure 15 can be applied to the PbO-based solvent, the reduction of Gd from x = 0.785 to x = 0.7 should lower the lattice parameter to that shown by the dotted line in Figure 16. The large discrepancy between the dotted and full line for $Gd_{0.7}Y_{1.55}Yb_{0.75}Ga_xFe_{5-x}O_{12}$ indicates that, for example, to maintain a given lattice parameter of 12.377Å, the Ga solution composition must be changed by ~ 1.8 % ($Ga_{0.51} \rightarrow Ga_{0.47}$) to maintain the same gallium content in the epitaxial films.

3.4. Film Thickness Measurement

Film thickness was measured by an optical interference technique shown in Figure 17. Nearly monochromatic radiation from a low pressure mercury lamp (λ = 5460Å) was reflected from the surface of the epitaxial layer with an angle of incidence θ, which was varied between 10° and 70° by rotating the sample. In this technique a portion of the incident beam passes through the epitaxial layer, is reflected off the substrate / epitaxial layer interface, and the resultant fringe pattern is observed at low magnification. The film thickness is obtained from the equation

$$h = \frac{\lambda}{m} \left[(n^2 - \sin^2 \theta_1)^{1/2} - (n^2 - \sin^2 \theta_2)^{1/2} \right]^{-1} \qquad (1)$$

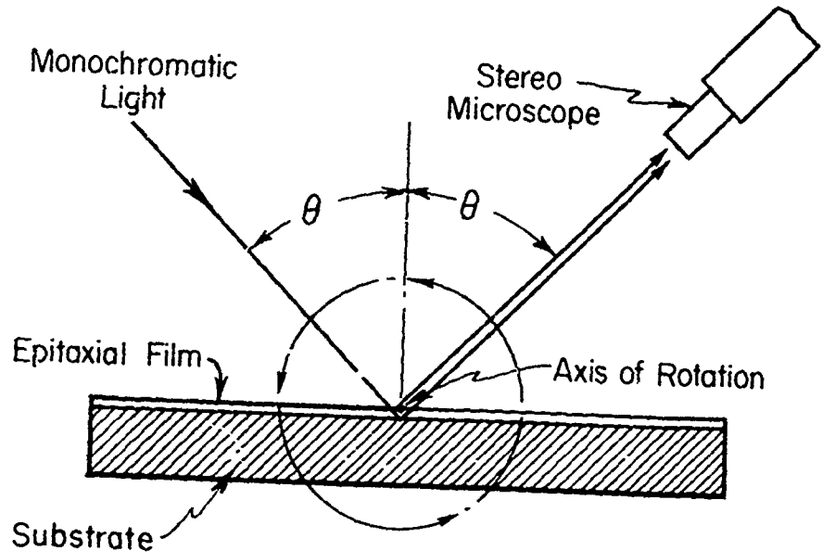

Figure 17. Apparatus for Measuring Film Thickness.

where n is the refractive index of the film, and $\theta_1-\theta_2$ is the change in the angle of incidence corresponding to m fringes passing through a particular reference point on the film. The refractive index n of the film is determined by placing a polarizer in the beam and measuring the Brewster angle θ_B, found by rocking the sample and observing the value of θ corresponding to minimum light reflection. The index of refraction is calculated from $n = \tan \theta_B$, and is typically 2.2 at $\lambda = 5460\mathring{A}$ for the $(Gd,Y,Yb)_3(Ga,Fe)_5O_{12}$ compositions measured. The reference point for the thickness measurement is chosen to be coincident with the axis of rotation of the sample, so that the reference point remains stationary when viewed through the microscope. Fringes pass through the reference point as θ is varied and move to regions of increasing thickness as θ is increased. By measuring values of θ for successive fringes moving through the reference point, the thickness of the film can be calculated with an accuracy of ±10%. The thickness variations over the whole surface of the film are recorded on a photograph of the film fringe pattern since each fringe corresponds to a difference in film thickness of about 0.13 μm. Typical fringe patterns are shown in Figure 18.

3.5. Static Domain Measurements

Magnetostatic theory was used to calculate the characteristic length ℓ and the saturation magnetization $4\pi M$ from the film thickness, bubble collapse field and stripe width using the equations devised by Bobeck.[27]

The wall energy σ_w and the anisotropy energy K_u can be calculated from the relation

$$\ell = \frac{\sigma_w}{4\pi M^2} = \frac{(AK_u)^{1/2}}{\pi M^2} \qquad (2)$$

where A is the exchange constant, assumed to have a value of about 4×10^{-7} ergs/cm.

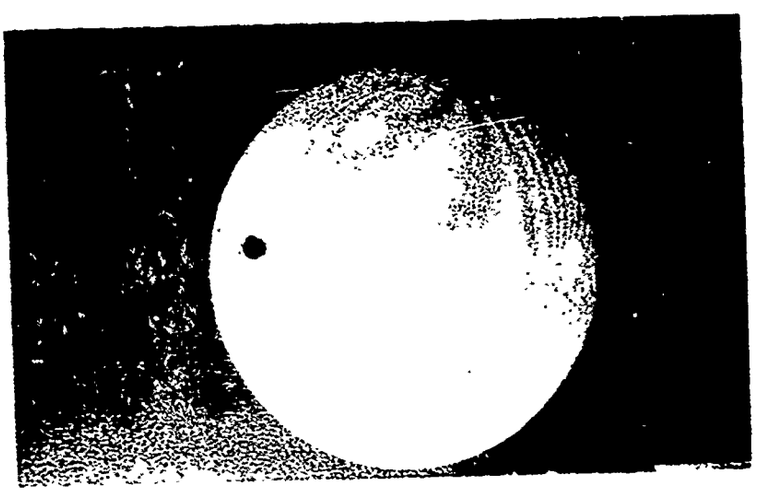

1mm

Figure 18. Typical fringe patterns in $(Gd,Y,Yb)_3(Fe,Ga)_5O_{12}$ 3.6 μm thick grown in $BaO-BaF_2-B_2O_3$ solvent. Na illumination (λ = 5890Å). The faint very narrow fringes near the center of the sample (if visible) are caused by interference between the front surface of the film and the back surface of the substrate.

3.6. Magnetization and Anisotropy Energy

$4\pi M$ and H_K were determined independently from torque magnetometer data. In this technique, the sample is held at 45° with respect to the applied field H by an optical-magnetic feedback system. The torque of the sample is cancelled by the torque produced by a current carrying coil in a permanent magnetic field. Since there are contributions to the torque from both the ferrimagnetic film and the paramagnetic substrate, a substrate correction is made from measurements of torque as a function of applied field H for both the substrate and substrate/film combination. A least-squares fit of the corrected torque data gives KV and MV where $H_K = 2K/M$, K is the anisotropy constant and V is the volume of the epitaxial film. The volume is estimated from thickness and area measurements, and H_K and $4\pi M$ can then be calculated and compared with the values determined from static domain measurements.

3.7. Domain Wall Mobility

3.7.1. Dynamic Bubble Collapse

Using this technique, the bubble diameter was first calculated as a function of applied field from the quantities σ/h and $4\pi M$. Bubbles of known diameter were then produced by application of a dc bias field H_b. A pulse field H_p was applied parallel to the bias field, and the pulse width τ was increased slowly until the bubble completely collapsed at τ_c. The τ_c data for several various values of H_b and H_p were used for the calculation of the mobility μ of collapsing bubbles by a mathematical fit to the exact solution of bubble stability according to Thiele.[28] Calculation

of the mobility μ involves the assumption of linearity of the domain wall velocity with the force required to collapse the bubble. Some of the films that have been examined appear to be nonlinear as evidenced by the constancy of τ_c as H_p substantially increased. For these specimens it appears that there is a velocity limit at large values of applied field, which has also been observed by other investigators.[29]

3.7.2. Stripe Domain Response to Applied Field

The experimental configuration for this method is shown in Figure 19. At zero bias field a pulse field H_p was applied so that the stripe width varied by only 10-20%. This resulted in essentially no variation in the stripe configuration Transmitted polarized light was modulated by the response of the stripe domains to the pulse field, and this modulation was detected as a voltage pulse from the photomultiplier. The signal was fed into a sampling scope and plotted on an X-Y recorder. If the domain response is linear with applied field, the observed response should be exponential with a time constant τ given by

$$\tau = \left[\mu \frac{\partial H_m}{\partial x}\right]^{-1} , \qquad (3)$$

where μ is the wall mobility and $\frac{\partial H_m}{\partial x}$ is the gradient of the magnetostatic

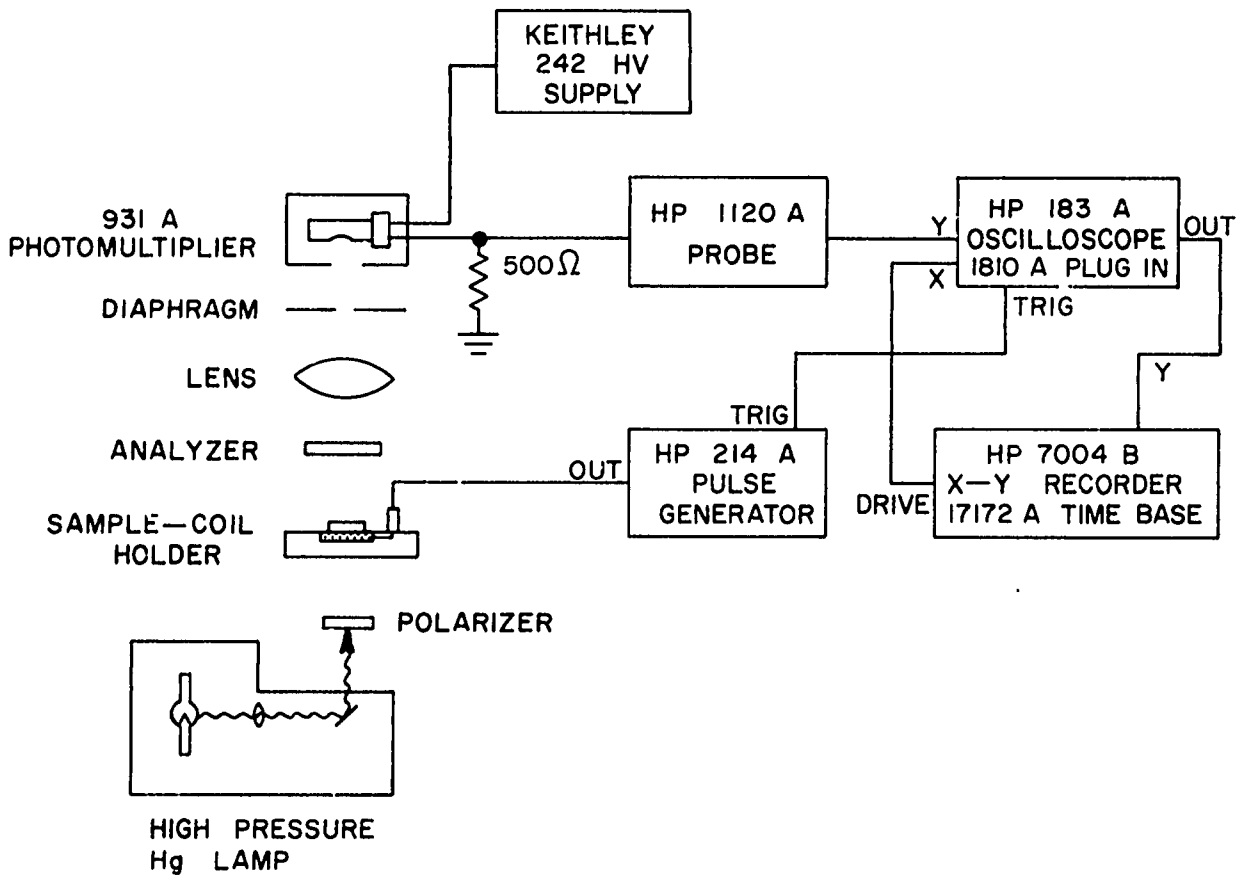

Figure 19. Experimental Configuration for Mobility Measurements.

field H_m which exists at each domain wall, and can be calculated from ℓ, h and $4\pi M$, using magnetostatic theory. The time constant τ can be derived from the observed response time of the signal by correcting for the rise time of the applied pulse field (~ 15 ns). If no such correction is made the calculated value of μ is lower than the true mobility.

Nonlinear velocity behavior of domain walls in response to the pulse field results in deviations from the expected exponential signal. The experiment reveals such nonlinearities in several garnet films, but it is difficult to analyze the data to extract the velocity versus drive field relationship. The results of mobility measurements are shown in Table VI.

3.8. Coercive Force

Two techniques were employed to measure the coercive force in the epitaxial films. The first is the familiar bubble repulsion technique in which the coercive force is given by the equation

$$H_c = \left(\frac{3\pi}{8}\right)\left(\frac{r^3 h}{d^4}\right)\left(4\pi M\right) \tag{4}$$

where r is the bubble radius, h is the film thickness and d is the equilibrium bubble spacing. The primary disadvantages of this technique are (i) H_c is a very strong function of r and d which are difficult to measure accurately; and (ii) localized pinning sites may prevent the bubble from moving freely, thus giving erroneously high values for the average coercive force.

TABLE VI

Properties of Epitaxial Layers Grown in $BaO-B_2O_3-BaF_2$ and $PbO-B_2O_3$ Solvents

Run Number	Solvent	Solution Composition	Thickness (μm) ±0.3μm	Lattice Parameter (Å) ±0.001Å	ℓ μm ±0.1	4πM (gauss) ±15%	H_K (Oe) ±10%	μ (cm/sec-Oe)	H_c (Oe) ±0.01 Oe	T_N (°C) ±1°C	ΔT_N (°C)	$\frac{\partial \ell}{\partial T}$ (μm/°C) ±0.5
RH4	$BaO-BaF_2$ B_2O_3	$EuEr_2Ga_{0.7}Fe_{4.3}O_{12}$	3	12.387	0.48	435	-	21	>1	-	-	-
LS88	"	$Gd_{0.7}Y_{1.55}Yb_{0.75}Ga_{0.9}Fe_{4.1}O_{12}$	2.1	12.370	0.68	160	720	>660	0.29	162	10	-
LS112	"	$Gd_{0.845}Y_{1.405}Yb_{0.75}Ga_{0.9}Fe_{4.1}O_{12}$	1.7	12.390	0.31	234	~ 300	>125	0.03	185	17.5	-
LS120	"	$Gd_{0.7}Y_{1.55}Yb_{0.75}Ga_{0.9}Fe_{4.1}O_{12}$	3.6	12.370	0.79	124	900	>680	0.1	163	7.5	-1.38
LS121	"	"	3.5	12.370	0.80	124	820	>350	0.05	164	8.7	-1.66
LS122	"	"	3.8	12.370	0.68	133	760	>420	0.05	164	7.5	-1.14
FP47	$PbO-B_2O_3$	$Gd_{0.785}Y_{1.465}Yb_{0.75}Ga_{0.45}Fe_{4.55}O_{12}$	3.1	12.379	0.96	117	800	>390	0.01	153	2.5	-0.7
FP57	"	$Gd_{0.7}Y_{1.55}Yb_{0.75}Ga_{0.4}Fe_{4.6}O_{12}$	2.8	12.381	0.23	260		>82	0.01	-	-	-
FP59	"	"	2.6	12.379	0.26	268		> 98	0.01	168	4.5	0 ± 0.1
FP62	"	$Gd_{0.7}Y_{1.55}Yb_{0.75}Ga_{0.46}Fe_{4.54}O_{12}$	4.5	12.380	0.73	127	640	>440	0.1	154	2.5	-0.509

The second technique involves AC modulation of a stripe domain pattern and gives a measure of the intrinsic coercive force of the film independent of localized defects. In this technique, shown schematically in Figure 20, a low frequency AC field $H_0 \sin \omega t$ is applied normal to the film. The stripe domain pattern in the film oscillates in response to the applied field as long as $H_0 > H_c$. The presence of coercivity causes distortion in the domain response and a phase shift in the response with repect to the applied AC field.

An optical signal proportional to the domain response is obtained as described in Section 3.7. A PAR lock-in detector is used to measure the in-phase ($F_1 \sin \omega t$) and quadrature ($F_2 \cos \omega t$) first harmonic components of the domain response as a function of H_0. One can show from theory that, as long as $H_0/H_c \geq 5$, $H_c \approx 0.82\ H_0 F_2/F_1$ is a good approximation. From the lock-in measurement, F_2/F_1 is easily determined and H_c is calculated, knowing H_0.

Utilizing this technique, coercive forces as low as 0.01 Oe can be measured. The method has the advantage that no magnetic parameters of the bubble materials appear in the calculation of H_c. The results of the coercive force measurements are shown in Table VI.

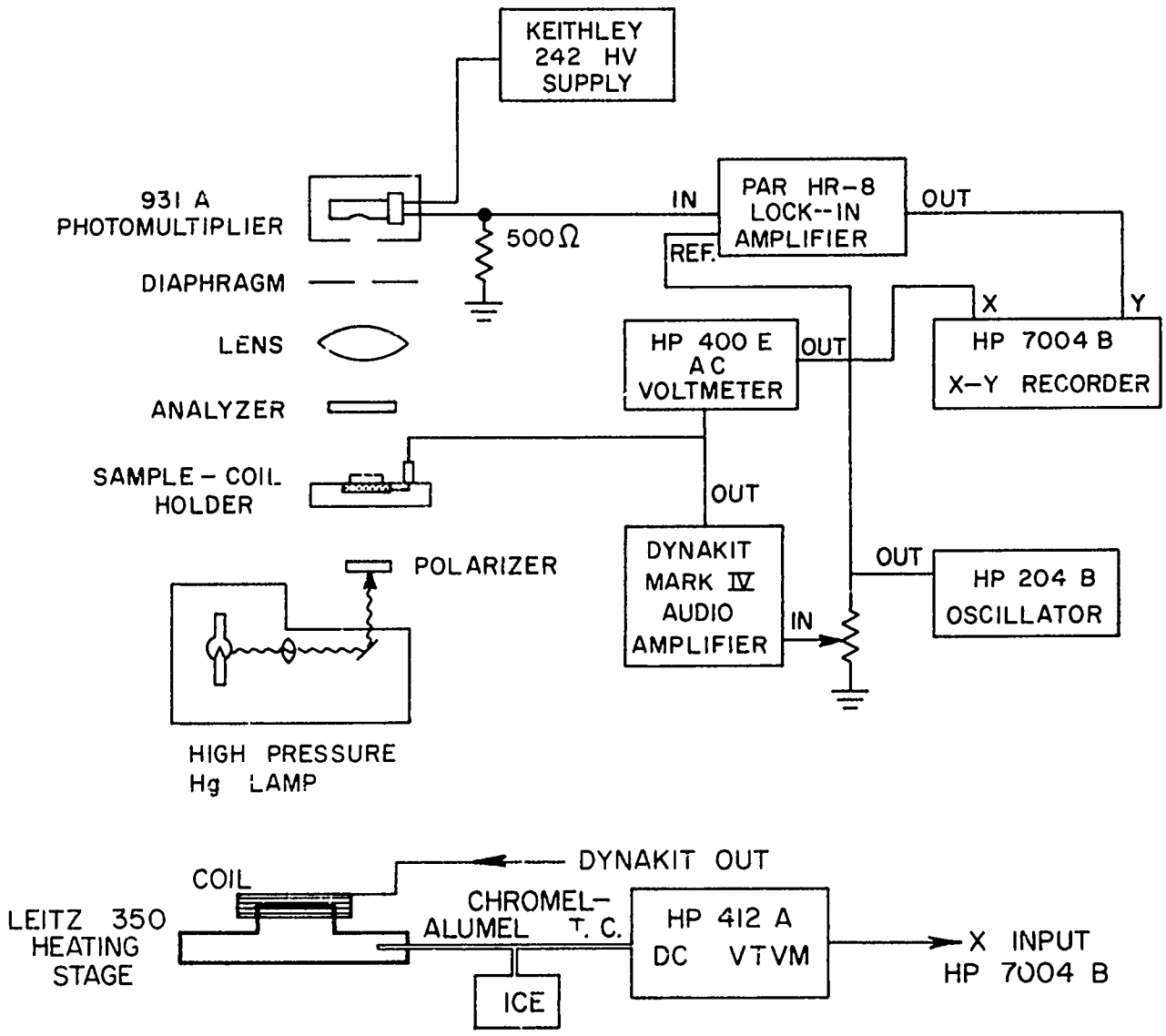

Figure 20. Apparatus for Coercive Force and Neél Temperature Measurements.

3.9. Neél Temperature Measurement

The Neél temperature is strongly dependent on the Fe/Ga ratio and only weakly dependent on the rare earth mixture in the garnet epitaxial layers. Measurement of the Neél temperature is, therefore, useful for determining the Ga content and monitoring the reproducibility of the film composition from run to run.

The apparatus used was the same as that used for the coercive force measurements (see Figure 20) with the exception that a hot stage replaced the sample-coil holder. The AC response of the stripe domain pattern was recorded as a function of temperature up to the Neél temperature at which the signal dropped sharply to zero. The results are shown in Table VI and Figure 21. Some of the specimens grown in the BaO-based solvent exhibit a transition region at the Neél temperature which consists of an initial sharp drop in the response followed by a more gradual decrease to zero.

This transition region was seen in the BaO-based solution for epitaxial layers grown isothermally at 990°C as well as for those grown by cooling from 1040°C to 990°C. In the PbO-based solution the temperature range of the transition is much narrower but is still detectable. The transition region may represent a Ga variation in the vertical direction in the epitaxial layers. However, since some of the narrowest regions in the BaO-based solvent were observed for the cooling runs, no correlation can be made between these observations and a possible change in Ga distribution coefficient with temperature in this solvent. Such a compositional variation would also be expected if the diffusion coefficients of Fe and Ga differed or if there were some meltback of the substrate before epitaxial growth

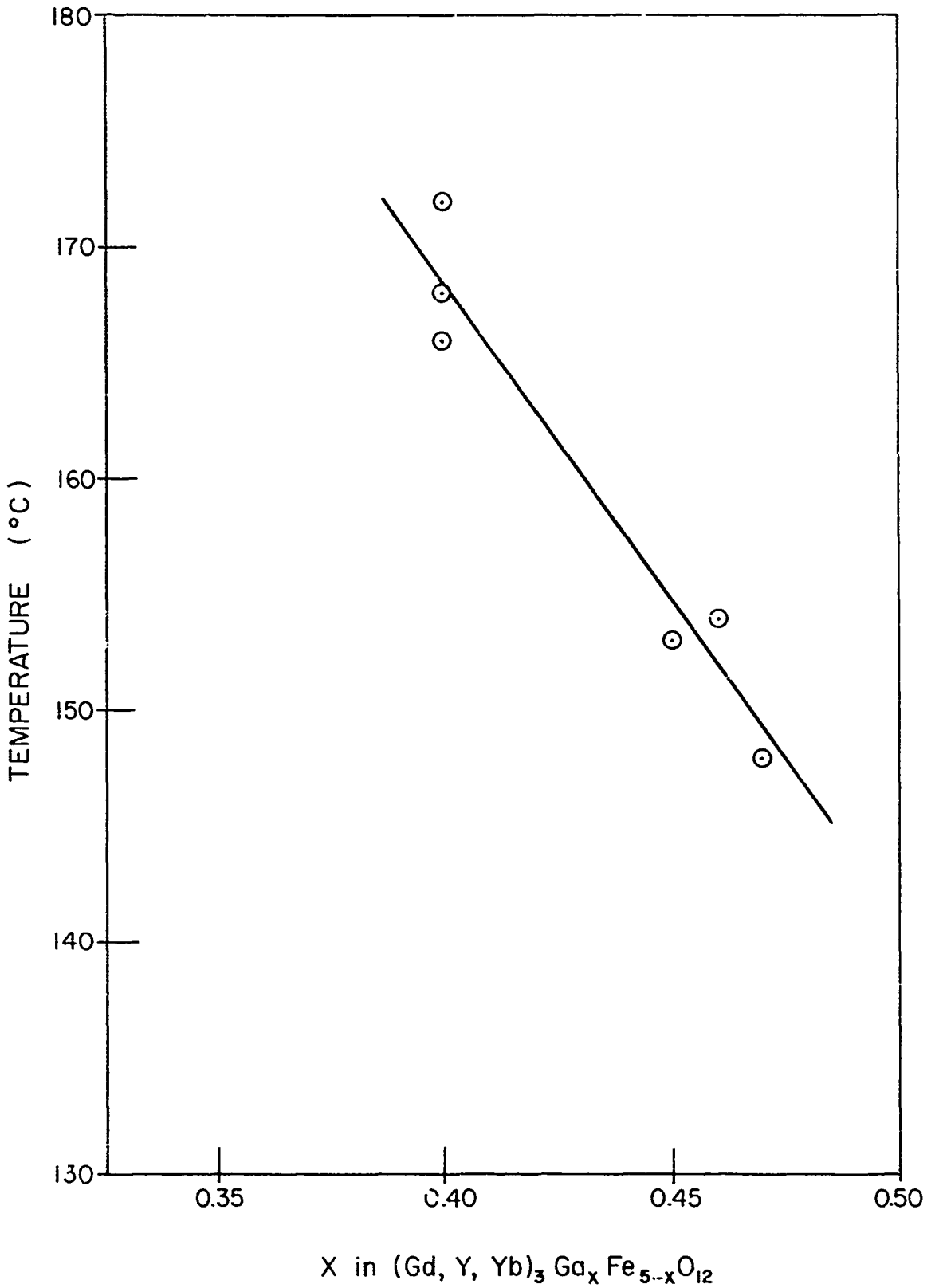

Figure 21. Neél temperature as a function of solution gallium content for $(Gd,Y,Yb)_3\ Ga_xFe_{5-x}O_{12}$ grown at 900°C in $PbO-B_2O_3$ solvent.

began. Then the composition of the layer would vary continuously through the initial transient period of crystal growth shown in Figure 9, followed by a region of constant composition after a steady-state condition was obtained. If this is the case, the width of the transition region should become narrower as the layer thickness increases, since there is less of a contribution from the initial transient region adjacent to the substrate. A possible trend of this type is indicated in Figure 22 for both the BaO-based and PbO-based solvents, although the scatter in the data prevents any firm conclusions to be drawn. It can be seen that the slope of the curves are about the same for the two solvents, but the magnitude of the transition region is consistently 3-4°C larger for the BaO-based solvent (except for the two anamolous points shown).

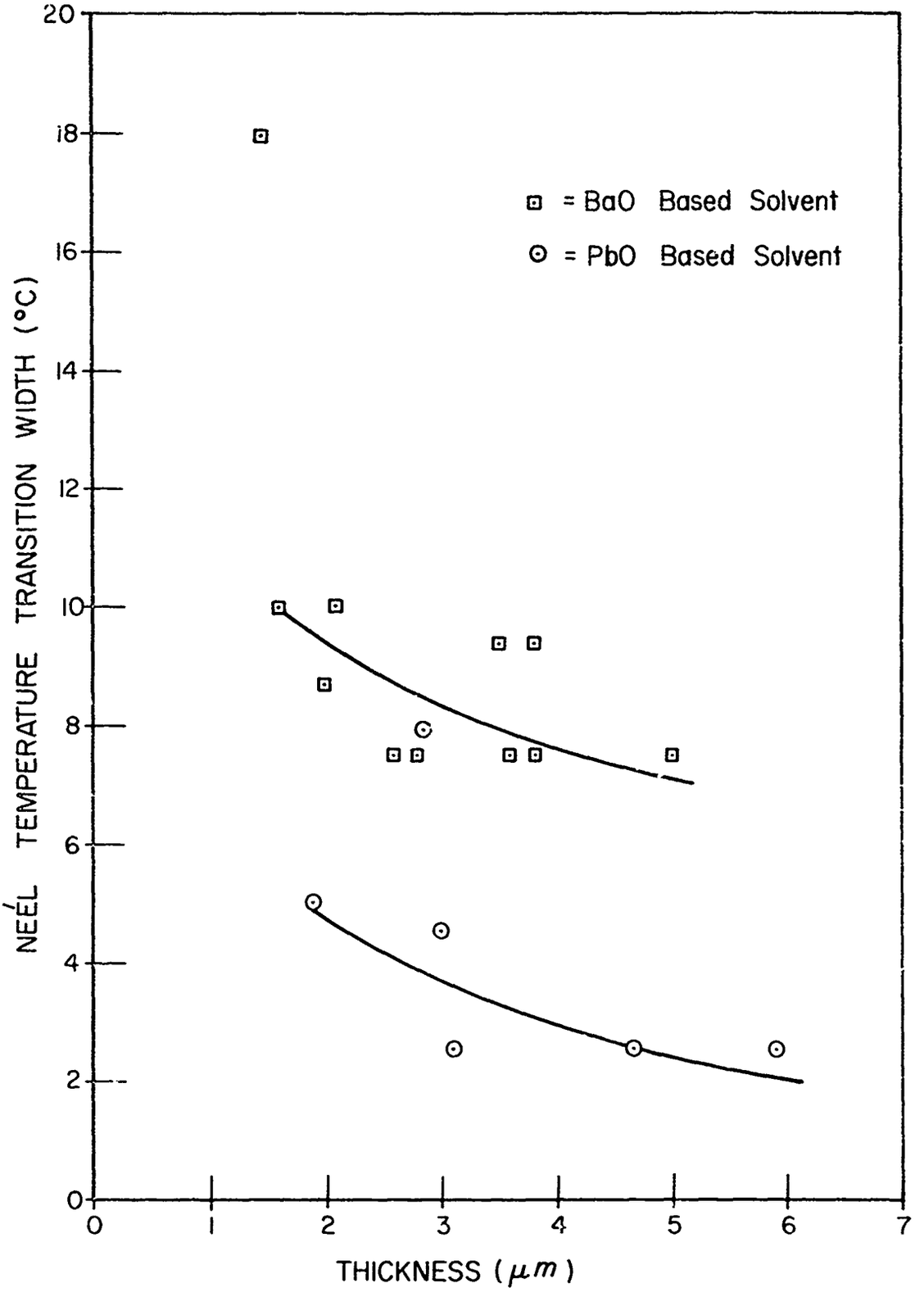

Figure 22. Variation of the Neél temperature transition region with epitaxial layer thickness.

3.10. Temperature Coefficient of Magnetic Properties

These measurements provide data for the determination of bubble stability with temperature, which is needed for establishing limits on ambient temperatures in operating devices. The specimen is placed in the hot stage shown in Figure 20 and the zero bias field stripe width as viewed through crossed polarizers is measured with a filar eyepiece. This measurement, coupled with the bubble collapse field as a function of temperature, which is measured in the same apparatus, gives the temperature coefficients of characteristic length, magnetization and anisotropy field. The temperature coefficient of characteristic length is given for a number of specimens in Table VI, and the temperature dependence of characteristic length, magnetization and the product of the exchange constant A times the anisotropy constant K are shown in Figures 23 and 24 for the composition $Gd_{0.7}Y_{1.55}Yb_{0.75}Ga_{0.9}Fe_{4.1}O_{12}$ grown in the BaO-based solvent.

The characteristic length (plotted as ℓ/h) is a monotonically decreasing function, while the magnetization has a maximum at ~ 90°C. The product of the exchange constant times the anisotropy constant also appears to be a monotonically decreasing function. Since for optimum device temperature stability, the characteristic length should be independent of temperature and $\ell = \frac{4(AK)^{1/2}}{4\pi M^2}$, it would be preferable to operate on the high temperature side of the maximum in $4\pi M$, which in this material is clearly at too high a temperature. It would be desirable from this standpoint, therefore, to adjust the composition to move this maximum to ~ 0°C.

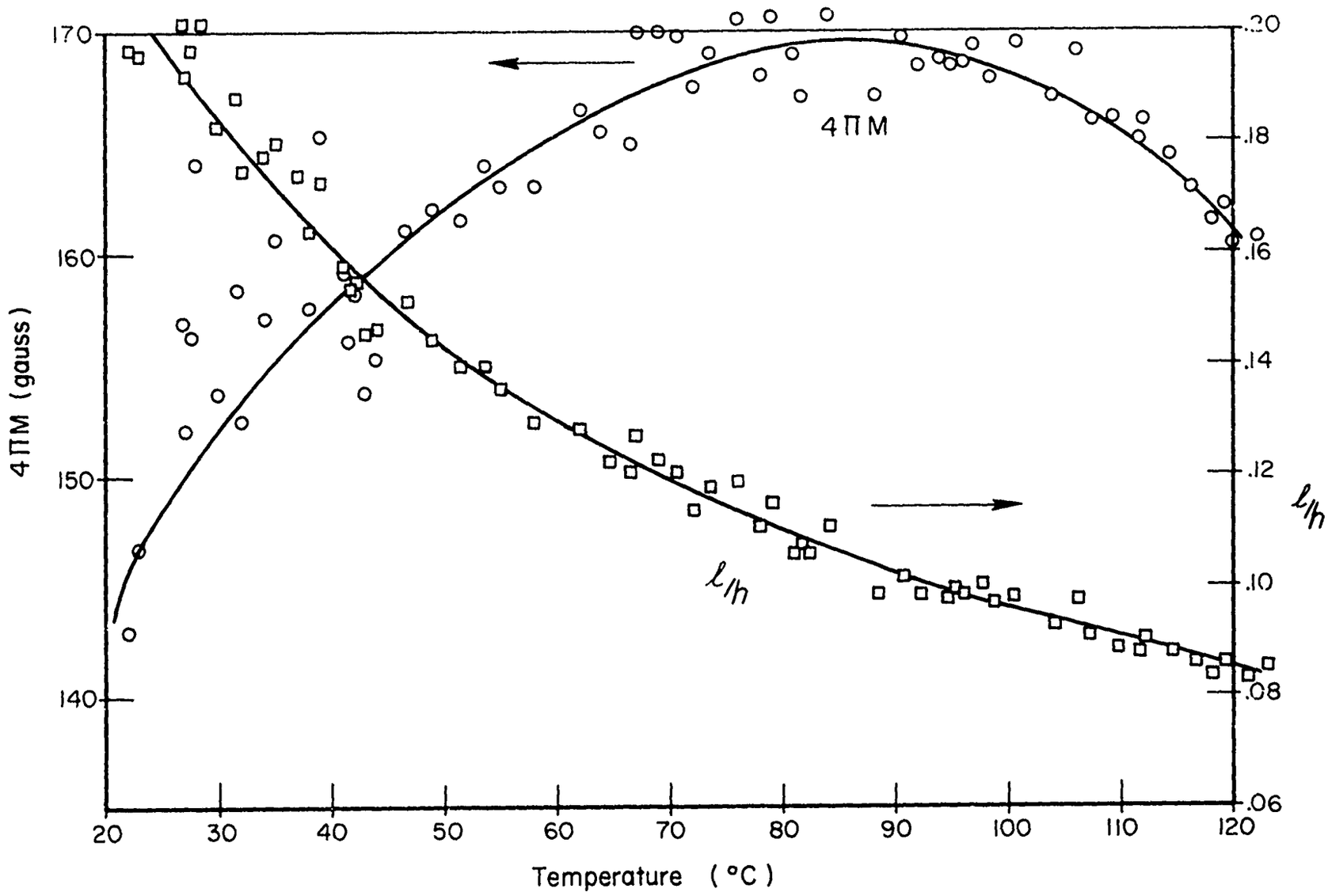

Figure 23. Temperature dependence of magnetization and characteristic length for $Gd_{0.7}Y_{1.55}Yb_{0.75}Ga_{0.9}Fe_{4.1}O_{12}$ grown in BaO-B_2O_3-BaF_2 solvent.

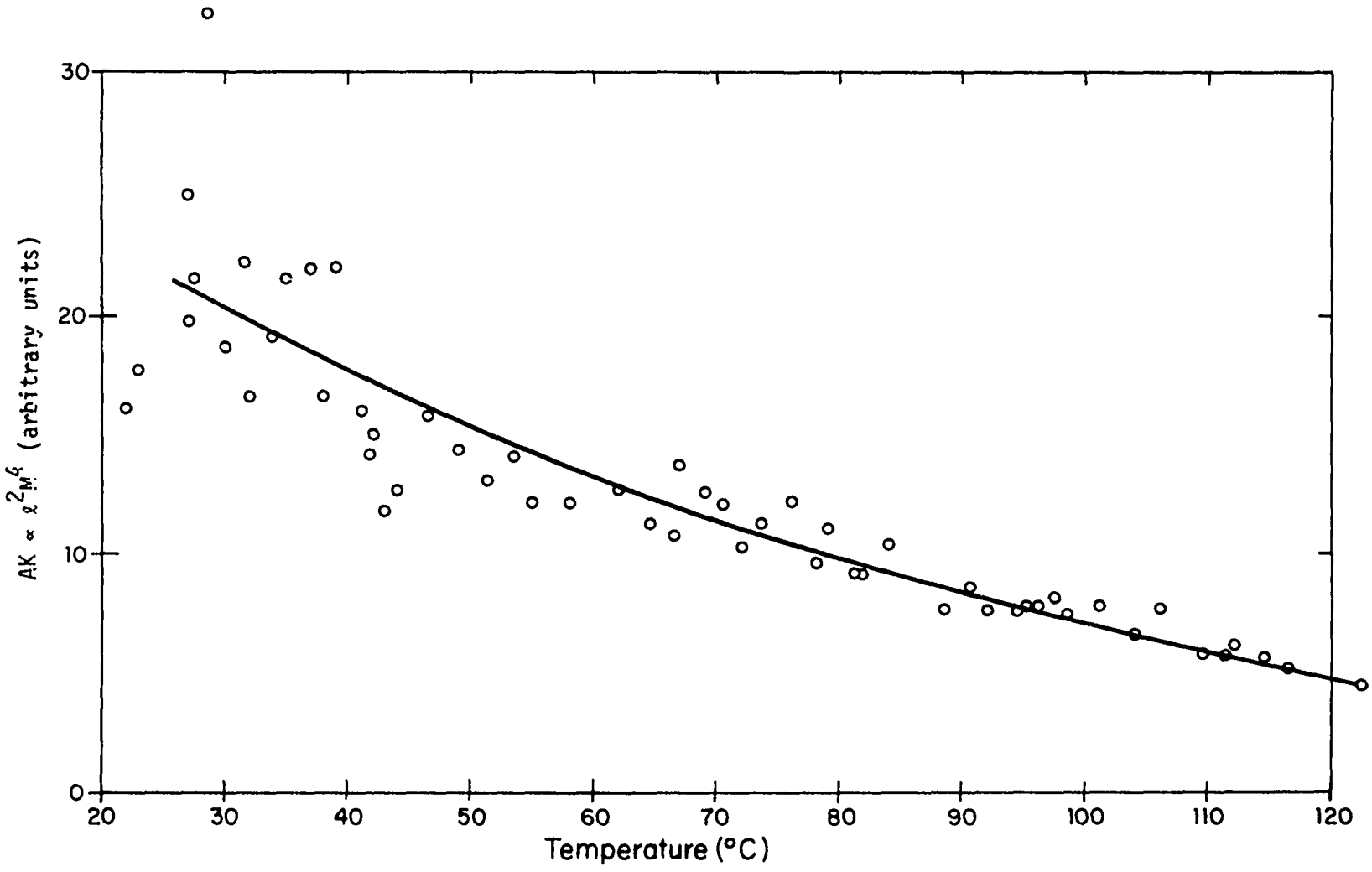

Figure 24. Temperature dependence of the product of the exchange constant A times the anisotropy constant K for $Gd_{0.7}Y_{1.55}Yb_{0.75}Ga_{0.9}Fe_{4.1}O_{12}$ grown in $BaO-B_2O_3-BaF_2$ solvent.

3.11. Results and Discussion of Magnetic Measurements

The results shown in Table VI indicate that the $(Gd,Y,Yb)_3$ $(Fe,Ga)_5O_{12}$ composition is superior to the $(Eu,Er)_3$ $(Ga,Fe)_5O_{12}$ garnets which were grown during the first phase of this contract. The most attractive composition to date is $Gd_{0.7}Y_{1.55}Yb_{0.75}Ga_{0.9}Fe_{4.1}O_{12}$, which satisfies all the requirements listed in Table I except the temperature coefficient of characteristic length. Bubbles in this material have been driven around a T-bar permalloy pattern at rates in excess of 5 kHz, and quasi-static operating margins for bubble propagation show that propagation can be achieved with an in-plane rotating drive field as low as 5 Oe, as shown in Figure 25.

The uniaxial anisotropy required for bubble domains is not an intrinsic property of the cubic garnets, and must be induced, either by preferential atomic ordering during the growth process or by stress caused by the lattice mismatch between the epitaxial layer and substrate. The origin of the anisotropy can be deduced from annealing experiments, since atomic diffusion will destroy the growth induced anisotropy. A sample of $Gd_{0.7}Y_{1.55}Yb_{0.75}$ $Ga_{0.9}Fe_{4.1}O_{12}$ was annealed for one hour at 1305°C, which eliminated nearly all of the uniaxial anisotropy so that the magnetization rotated into the plane due to magnetostatic forces. This indicates that the uniaxial anisotropy is primarily growth induced for this composition even though the lattice mismatch between the film and substrate is 0.012Å, a result which may be expected from the small calculated value of the magnetostriction coefficient $\lambda_{111} \sim -3 \times 10^{-6}$.

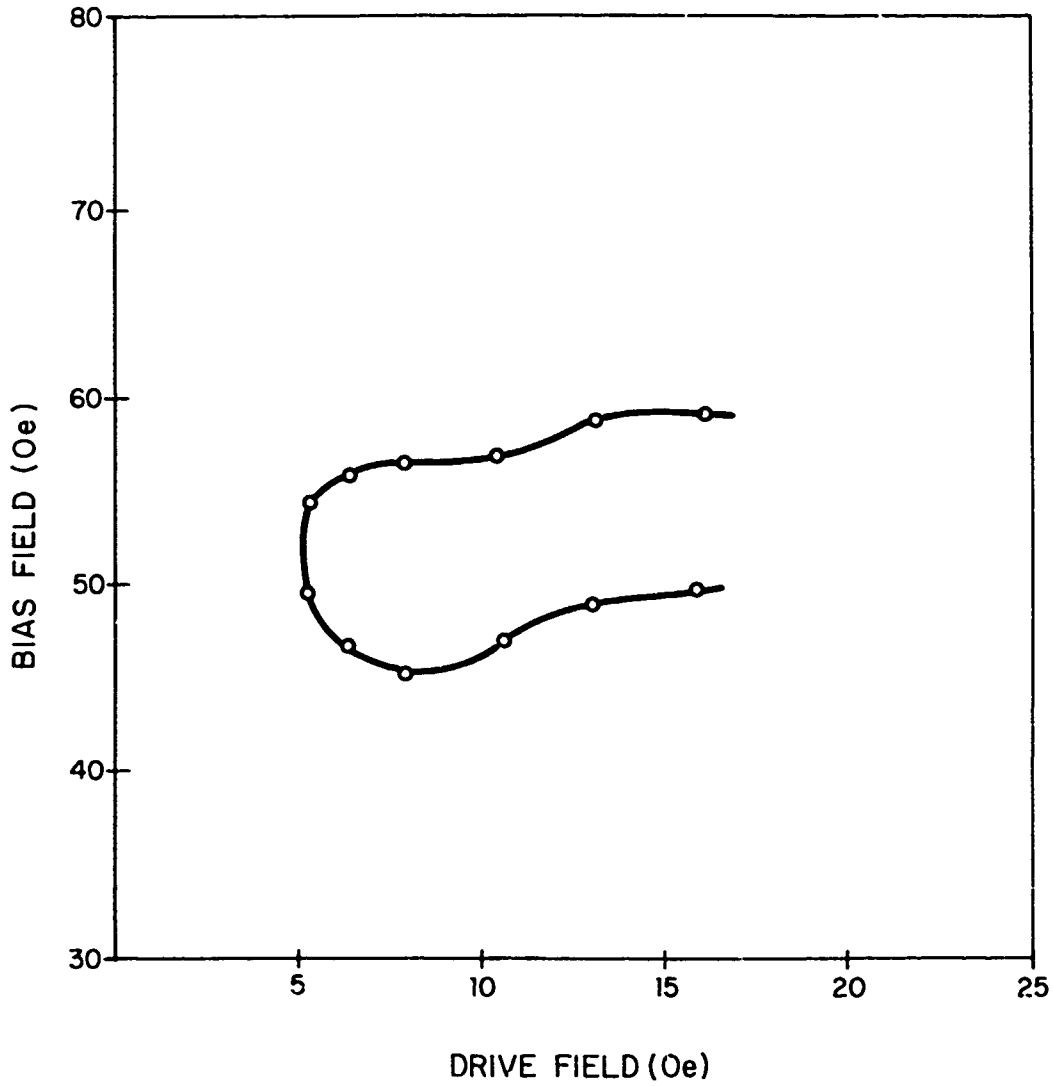

Figure 25. Quasi-static operating margins for $Gd_{0.7}Y_{1.55}Yb_{0.75}Ga_{0.9}Fe_{4.1}O_{12}$ Grown in $BaO-B_2O_3-BaF_2$ Solvent. (3μm spacing between T-bars and garnet surface).

Preliminary investigations do not indicate any striking differences in the quality of films grown in the PbO-based and BaO-based solvents, although detailed comparisons have not yet been completed. A summary of the properties of two films of nominally the same composition grown in the two solvents is shown in Table VII. The lower Neél temperature for the film grown in the $PbO-B_2O_2$ solvent indicates a slightly higher Ga content than for that grown in the BaO-based solvent. The large difference in lattice parameters can be attributed to the presence of ~ 0.7 wt % lead in the film grown in $PbO-B_2O_3$ (from Figure 14), which should increase the lattice parameter by ~ 0.01Å.[12] It is interesting to note that the presence of this impurity does not appreciably degrade the magnetic properties of the epitaxial layer. The most significant difference in the two films is the width of the transition region at the Neél temperature, which is consistently higher for the BaO-based solvent. These data are indicative of a greater variation in the Ga/Fe ratio normal to the growth interface in this solvent, which may arise from several sources as discussed in Section 3.9.

Perhaps the most interesting phenomenon seen in films of $(Eu,Er)_3(Ga,Fe)_5O_{12}$ and $(Gd,Y,Yb)_3(Ga,Fe)_5O_{12}$ grown both in the PbO-based and BaO-based solvents is the existence of a new type of bubble termed the "hard bubble,"[30] which has properties quite different from the standard bubble domain described by Thiele's theory. Both types of bubbles can be formed from stripe domains by cutting these domains with a localized pulsed magnetic field produced by a coil placed close to the garnet film. Simply pinching off the end of a domain invariably produces a Thiele type bubble. If, however, the stripe domains are in a state of turbulence when they are cut, it is possible to produce not only Thiele type bubbles, but also up to 20% of the hard bubbles.

TABLE VII

Comparison of the Properties of Rare Earth Bubble Garnets Grown in BaO-Based and PbO-Based Solvents

Parameter	BaO-based Solvent	PbO-based Solvent
Run Number	LS120	FP62
Solution Composition	$Gd_{0.7}Y_{1.55}Yb_{0.75}Ga_{0.9}Fe_{4.1}O_{12}$	$Gd_{0.7}Y_{1.55}Yb_{0.75}Ga_{0.46}Fe_{4.54}O_{12}$
Nominal Solid Composition	"	$Gd_{0.7}Y_{1.55}Yb_{0.75}Ga_{0.9}Fe_{4.1}O_{12}$
Run Temperature	1040 → 990°C	900 ±0.3°C
Run Time	21.8 min.	15 min.
Lattice Parameter	12.370 ±0.001Å	12.380 ±0.001Å
Thickness at Center	3.6 ±0.1 μm	4.5 ±0.1μm
Thickness variation over Central Area (~ 1 cm^2)	< ±0.15μ	< ± 1μm
Maximum Defect Free Area	> 10 mm^2	~ 10 mm^2
Characteristic Length	0.8 ±0.05 μm	0.73 ±0.05 μm
Magnetization	124 ±10 gauss	127 ±10 gauss
Anisotropy Energy	910 ±80 Oe	640 ±80 Oe
Mobility	> 680 cm/Oe-sec	> 440 cm/Oe-sec
Coercive Force	< 0.05 Oe	< 0.05 Oe
Neél Temperature	163 ±1°C	154 ±1°C
Neél Temperature Transition Width	7.5 ±0.3°C	2.5 ±0.3°C

These hard bubbles obey a different diameter versus bias field relationship compared with the Thiele bubble as shown in Figure 26. They are stable to a higher applied field and a smaller diameter than the Thiele bubbles (produced in the same area of the same film). There is a range of bias fields for which only the hard bubbles are stable, and therefore there is the possibility of using these bubbles in devices. We have propagated hard bubbles on a T-bar pattern and obtained quasi-static propagation for a 30% variation of the bias field compared to 15-20% for Thiele type bubbles.

A series of photographs taken of Thiele and hard domains in $Gd_{0.7}Y_{1.55}Yb_{0.75}Ga_{0.9}Fe_{4.1}O_{12}$ grown in the BaO-based solvent is shown in Figure 27. After the stripe domains have been cut and the bias field is increased, first the Thiele type domains collapse, leaving a variety of different types of hard bubbles as evidenced by the striking difference in diameter of the bubbles in Figures 27b-27e. As the bias field is decreased, the hard bubbles tend to strip out in a spiral pattern as shown in Figure 27f, rather than linearly as predicted by magnetostatics.

The observed behavior of hard bubbles is consistent with the following proposed model. Hard bubbles may have a domain wall energy σ_w which decreases with bubble radius. If this is true, then as H increases, ℓ decreases, h/ℓ increases and, according to Thiele theory, $H_{collapse}$ increases. Thus, as H increases, the hard bubbles may exist at smaller diameters and higher fields, compared with a domain for which σ_w is independent of field and bubble radius.

As the bias field is decreased, hard bubbles always strip out in a spiral rather than as a linear stripe. If σ_w is reduced by reducing the radius of curvature of the domain wall, as implied above, the spiral structure would be expected for a wide range of magnetostatic conditions.

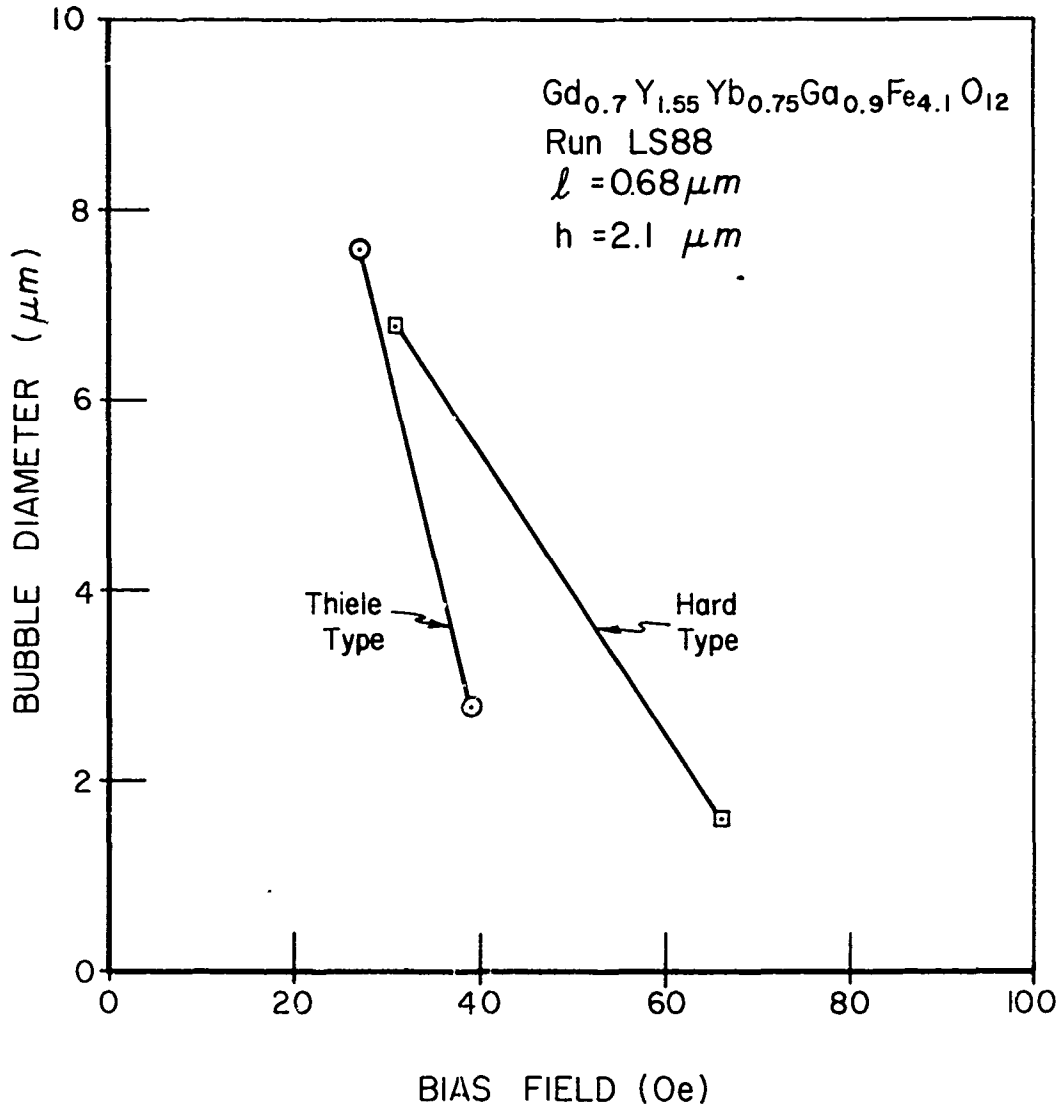

Figure 26. Dependence of bubble diameter upon bias field for Thiele type and hard type bubbles.

Figure 27a. Domain structure in $Gd_{0.7}Y_{1.55}Yb_{0.75}Ga_{0.9}Fe_{4.1}O_{12}$. Zero bias field (200X).

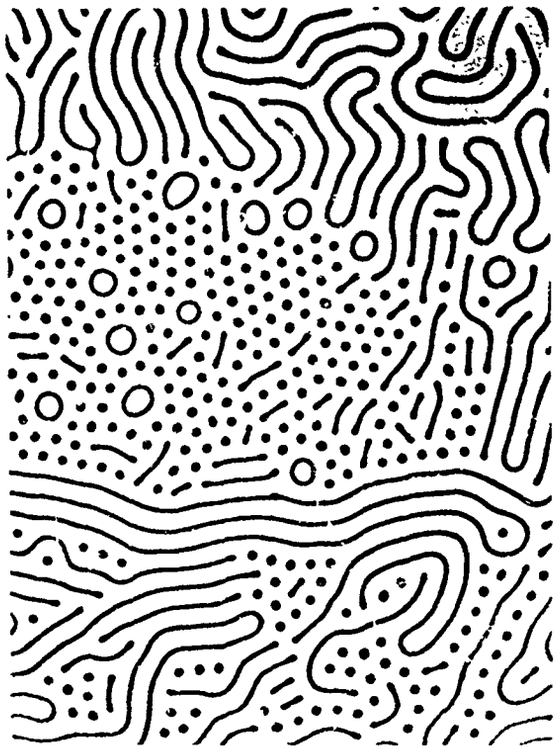

Figure 27b. Domains have been cut and bias field increased to 20 Oe. (200X)

Figure 27c. Bias field 30 Oe. (200X)

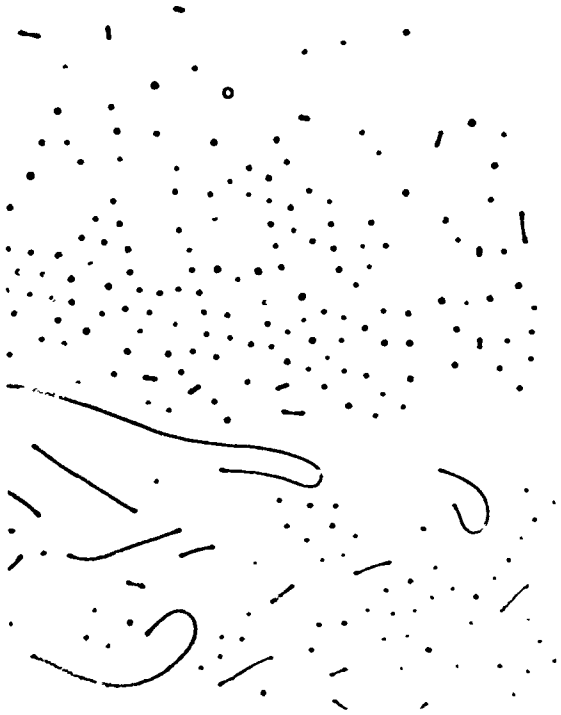

Figure 27d. Bias field 40 Oe (200X)

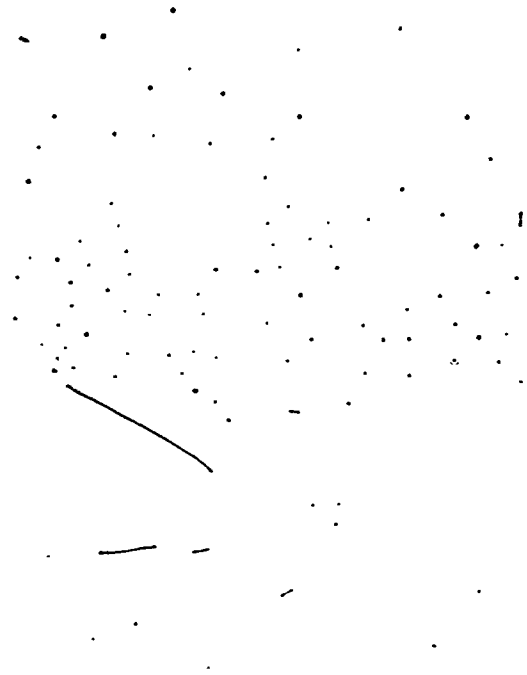

Figure 27e. Bias field 53 Oe (200X)

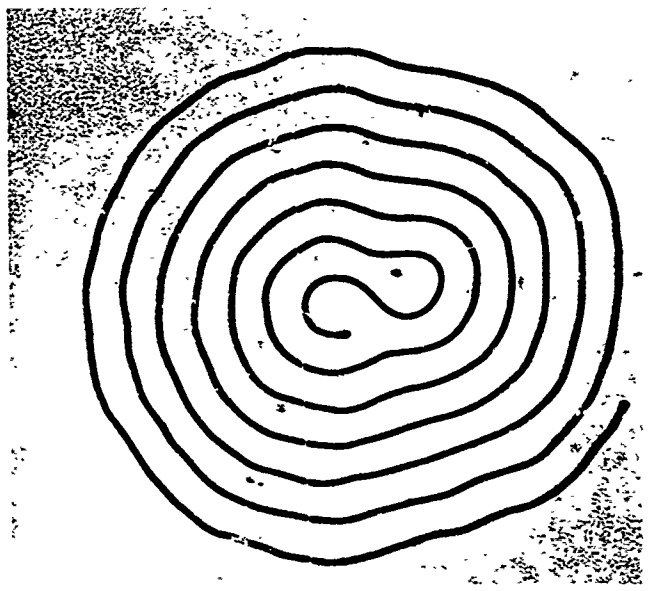

Figure 27f. Bias field increased to 65 Oe tc pop most bubbles, then reduced to 28 Oe. (200X)

A domain wall structure which gives a wall energy dependent on radius of curvature is easy to hypothesize. The domain walls of hard bubbles may have successive sections of right handed and left handed Bloch walls as shown in Figure 28a. The energy of discontinuity can be reduced by the formation of a Neél wall as shown in Figure 28b. This is not the only possible wall structure, however. The energy of the discontinuity is also reduced by reducing the radius of curvature of the wall as shown in Figure 28c, i.e., what was a 180° disruption in spin alignment across the discontinuity is reduced to less than 180° by bending the wall. Thus σ_w would be expected to decrease with radius of curvature. The number of such discontinuities around the circumference probably varies, depending on the manner in which the stripe domains are cut initially. The number of discontinuities determines the total energy of the wall and a range of hard bubbles with different properties is expected, as shown in the photographs.

The above model is consistent with the experimental behavior of hard bubble domains, but the model requires verification. A mathematical formulation of the energetics of discontinuous Bloch walls is desirable. A direct observation of the wall structure does not seem possible. At this time, it is not clear whether the hard bubbles are desirable or detrimental to device operation, but this is not a serious problem since they can be produced or eliminated at will by proper selection of the bubble generation method.

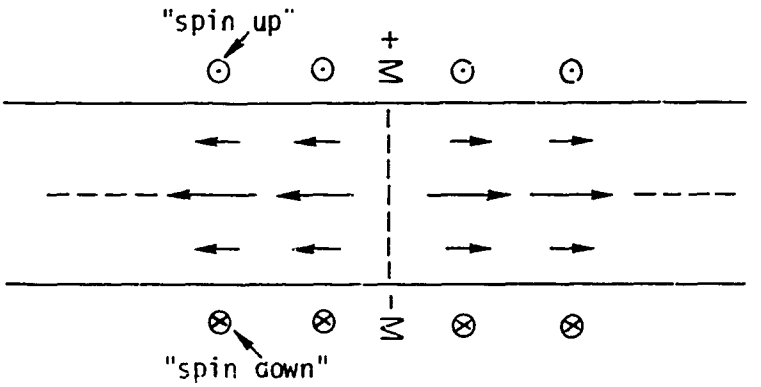

(a) Discontinuity at the junction of a right-handed and left-handed Bloch wall

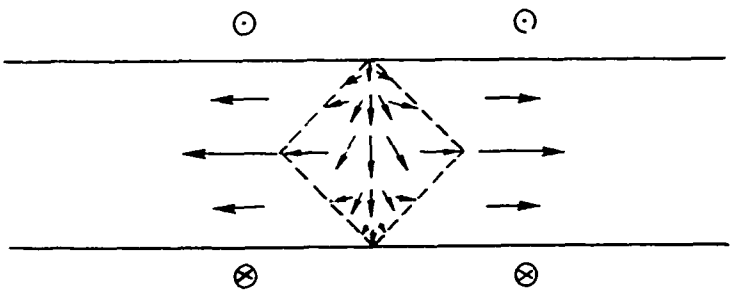

(b) Neél wall which reduces the energy of the above discontinuity.

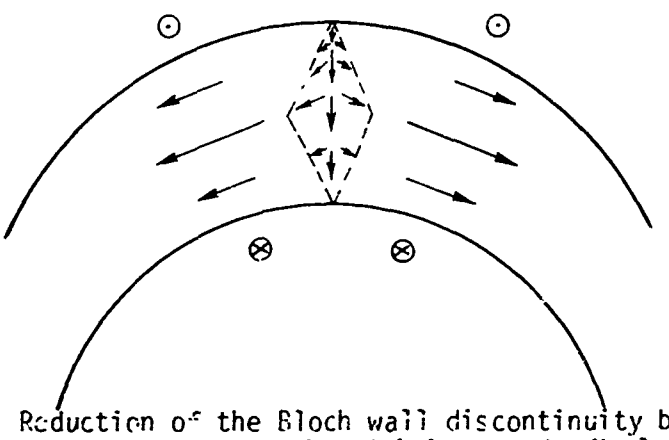

(c) Reduction of the Bloch wall discontinuity by introduction of wall curvature in addition to the Neél wall.

Figure 28. Proposed model for the domain wall structure of hard bubbles. Arrows represent the component of spin in the plane of a bubble film.

SECTION IV

4.0. CONCLUSIONS

Controlled and reproducible liquid phase epitaxial growth of the rare earth garnets $(Eu,Er)_3(Ga,Fe)_5O_{12}$ and $(Gd,Y,Yb)_3(Ga,Fe)_5O_{12}$ on $Gd_3Ga_5O_{12}$ substrates has been demonstrated in the BaO-based solvent. This solvent, comprised of $BaO-B_2O_3-BaF_2$, has been characterized with respect to relevant phase equilibria and rare earth garnet solubility, and suitable growth parameters for the growth of the rare earth garnets have been developed.

The above compositions have also been grown in the commonly used $PbO-B_2O_3$ solvent to provide a basis of comparison between the two solvents. These films have been characterized with respect to composition, defect density and distribution, lattice parameters, thickness uniformity and magnetic properties. Initial results indicate that films of nominally the same composition grown in the two solvents at different temperatures are of comparable quality, although control of the reproducibility is considerably easier with the BaO-based solvent.

The optimum garnet composition found to date has been $Gd_{0.7}Y_{1.55}Yb_{0.75}Ga_{0.9}Fe_{4.1}O_{12}$ (solution composition in the BaO-based solvent), which meets all the device specifications except that of temperature stability. Annealing experiments indicate that the uniaxial anisotropy is primarily growth induced in this material. Bubbles have been driven around a T-bar pattern at rates exceeding 5 kHz and quasistatic operating margins for bubble propagation show that propagation can be achieved with an in-phase rotating field as low as 5 Oe.

REFERENCES

1. A. H. Bobeck, Bell System Tech. J. 46, 1901 (1967).

2. L. G. Van Uitert, W. A. Bonner, W. H. Grodkiewicz, L. Pictroski and G. J. Zydzik, Mat. Res. Bull. 5, 825 (1970).

3. R. A. Burmeister, T. L. Felmlee and R. Hiskes, Semiannual Technical Report, Magnetic Rare Earth Compounds Contract No. DAAH01-70-C-1106 December, 1970.

4. R. A. Burmeister, T. L. Felmlee and R. Hiskes, Final Technical Report, Magnetic Rare Earth Compounds, Contract No. DAAH01-70-C-1106, June, 1971.

5. R. A. Burmeister and R. Hiskes, Semiannual Technical Report, Magnetic Rare Earth Compounds II, Contract No. DAAH01-71-C-1259, February, 1972.

6. J. W. Nielsen, Met. Trans. 2, 625 (1971).

7. L. K. Shick, J. W. Nielsen, A. H. Bobeck, A. J. Kurtzig, P. C. Michaelis and J. P. Reekstin, Appl. Phys. Letters 18, 89 (1971).

8. R. C. Linares, R. B. McCraw and J. B. Schroeder, J. Appl. Phys. 36, 2884 (1965).

9. R. C. Linares, J. Cryst. Growth 3,4 443 (1968).

10. H. J. Levinstein, S. Licht, R. W. Landorf and S. L. Blank, Appl. Phys. Letters 19, 486 (1971).

11. E. A. Giess, B. A. Calhoun, E. Klokholm, T. R. McGuire and L. L. Rosier, Mat. Res. Bull. 6, 317 (1971).

12. E. A. Giess, B. E. Argyle, D. C. Cronemeyer, E. Klokholm, T. R. McGuire, D. F. O'Kane, T. S. Plaskett and V. Sandagopan, AIP Conference Proceedings No. 5, Magnetism and Magnetic Materials Conference 1971, edited by C.D. Graham, Jr. and J. J. Rhyne, American Institute of Physics, New York, 1972

13. H. H. Quon and A. J. Potvin, Mat. Res. Bull, 7, 463 (1972).

14. R. Hiskes, T. L. Felmlee and R. A. Burmeister, to be published in J. Electronic Materials.

15. D. M. Heinz, P. J. Besser, P. E. Elkins, H. L. Glass, J. E. Mee and L. A. Moudy, Technical Report AFML-TR-71-126, June 1971.

16. R. Zeytang, J. Appl. Phys. 41, 3718 (1970).

17. D. M. Heinz, P. J. Besser, J. M. Owens, J. E. Mee and G. R. Pulliam, J. Appl. Phys. 42, 1243 (1971).

18. J. E. Mee, G. R. Pulliam, D. M. Heinz, J. M. Owens and P. J. Besser, Appl. Phys. Letters 18, 60 (1971).

19. J. E. Mee, P. J. Besser and F. A. Pizzarello, Technical Report AFAL-TR-70-194, Sept. ,1970.

20. J. E. Mee, P. J. Besser, P. E. Elkins H. L. Glass and E. C. Whitcomb, Technical Report No. NAS 12-522, February, 1972.

21. D. C. Miller, Electrochemical Society Meeting,Houston, Texas, May 1972.

22. J. Basterfield, M. J. Prescott, and B. Cockayne, J. Mater. Sci. 3, 33 (1968).

23. H. L. Glass, Mat. Res. Bull. 7, 385 (1972).

24. L. J. Varnerin, Jr., presented at INTERMAG 72, Kyoto, Japan, April, 1972.

25. G. P. Espinosa, J. Chem. Phys. 37, 2344 (1962).

26. L. Pauling, "The Nature of the Chemical Bond," Cornell University Press, Cornell, New York, 1960.

27. A. H. Bobeck, R. F. Fischer, A. J. Perneski, J. P. Remeika and L. G. Van Uitert, IEEE Trans. on Magnetics MAG-5, 544 (1969).

28. A. A. Thiele, Bell System Tech. J. 48, 3287 (1969).

29. B. A. Calhoun, E. A. Giess and L. L. Rosier, Appl. Phys. Letters 18, 287 (1971).

30. A. H. Bobeck,presented at the Electrochemical Society Meeting, Houston,Texas, May, 1972.